Button, D. J., Barrett, P., & Rayfield, E. (2016). Comparative cranial myology and biomechanics of *Plateosaurus* and *Camarasaurus* and evolution of the sauropod feeding apparatus. *Palaeontology*, *59*(6), 887-913. https://doi.org/10.1111/pala.12266

University of Bristol - Explore Bristol Research
General rights

COMPARATIVE CRANIAL MYOLOGY AND BIOMECHANICS OF *PLATEOSAURUS* AND *CAMARASAURUS* AND EVOLUTION OF THE SAUROPOD FEEDING APPARATUS

by DAVID J. BUTTON[1,2,3], PAUL M. BARRETT[2] *and* EMILY J. RAYFIELD[1]

[1]School of Earth Sciences, University of Bristol, Life Sciences Building, 24 Tyndall Avenue, Bristol, BS8 1TQ, UK; e.rayfield@bristol.ac.uk
[2]Department of Earth Sciences, The Natural History Museum, London, SW7 5DB, UK; p.barrett@nhm.ac.uk
[3]*Current address*: School of Geography, Earth and Environmental Sciences, University of Birmingham, Edgbaston, Birmingham, B15 2TT, UK; d.j.button@bham.ac.uk

Abstract: Sauropodomorpha represents an important group of Mesozoic megaherbivores, and includes the largest terrestrial animals ever known. It was the first dinosaur group to become abundant and widespread, and its members formed a significant component of terrestrial ecosystems from the Late Triassic until the end of the Cretaceous. Both of these factors have been explained by their adoption of herbivory, but understanding the evolution of sauropodomorph feeding has been hampered by the scarcity of biomechanical studies. To address this, the jaw adductor musculature of the basal sauropodomorph *Plateosaurus* and the sauropod *Camarasaurus* have been reconstructed. These reconstructions provide boundary conditions for finite element models to assess differences in structural performance between the two taxa. Results demonstrate that *Camarasaurus* was capable of much greater bite forces than *Plateosaurus*, due to greater relative adductor muscle mass and shape changes to the mandible. The skull and mandible of *Camarasaurus* are also 'stronger' under static biting. The *Plateosaurus* mandible appears to compromise structural efficiency and force transmission in order to maintain relatively high jaw closure speed. This supports suggestions of facultative omnivory in basal sauropodomorph taxa. The expanded mandibular symphysis and 'lateral plates' of sauropods each lead to greater overall craniomandibular robustness, and may have been especially important in accommodating forces related to asymmetric loading. The functional roles of these characters, and observed general shape changes in increasing skull robustness, are consistent with hypotheses linking bulk-herbivory with the origin of Sauropoda and the evolution of gigantism.

Key words: Sauropodomorpha, finite element analysis, herbivory, palaeoecology, biomechanics, virtual reconstruction.

SAUROPODOMORPHA represents one of the most important Mesozoic terrestrial herbivore groups, numbering more than 200 genera and occupying all continents (Galton & Upchurch 2004; Upchurch *et al.* 2004; Weishampel *et al.* 2004; Mannion *et al.* 2011; Sander 2013). This clade includes the sauropods, the largest terrestrial animals known, with taxa commonly exceeding 20 tonnes in body mass (Klein *et al.* 2011; Benson *et al.* 2014) and the largest reaching in the region of 60–70 tonnes (Mazzetta *et al.* 2004; Lacovara *et al.* 2014; but see Bates *et al.* 2015). The extreme nature of sauropodomorph biology makes exploration of their functional anatomy and evolution imperative for understanding the constraints acting upon terrestrial life (Clauss 2011; Sander *et al.* 2011; Sander 2013).

The skull forms a fundamental link between an animal and its environment, especially through feeding. Feeding behaviour influences all parts of an animal's lifestyle, including life history strategy, energetics, habitat preference and ecological role (e.g. Owen-Smith 1988; Chapman & Reiss 1999; Schwenk 2000). In turn, information on feeding in prehistoric animals can inform larger evolutionary patterns (Reisz & Sues 2000; Barrett & Rayfield 2006; Barrett 2014). Although the small size and superficial simplicity of the sauropod skull perplexed earlier authors (e.g. Hatcher 1901; Haas 1963; Colbert 1993) it is now known that the sauropod skull represents a specialized cropping tool (Christiansen 1999; Upchurch & Barrett 2000; Sereno *et al.* 2007; Hummel & Clauss 2011; Sander *et al.* 2011; Young *et al.* 2012; Sander 2013). Multiple studies of craniodental functional anatomy (e.g. Barrett & Upchurch 1994, 2005, 2007; Calvo 1994; Christiansen 1999, 2000; Upchurch & Barrett 2000) have

provided insights into sauropodomorph ecology and evolution, although quantitative biomechanical analyses (Preuschoft & Witzel, 2005; Witzel *et al.* 2011; Young *et al.* 2012; Button *et al.* 2014) have been rarer.

The ability to eat plants has been implicated in the early diversification of Sauropodomorpha (Galton 1985*a*; Barrett & Upchurch 2007; Barrett *et al.* 2011) and the evolution of the sauropod feeding apparatus (Barrett & Upchurch 2007; Upchurch *et al.* 2007; Sander & Clauss 2008; Sander *et al.* 2011; Sander 2013). Adoption of obligate high-fibre herbivory and bulk-feeding are seen as integral drivers of sauropod gigantism (Barrett & Upchurch 2007; Upchurch *et al.* 2007; Yates *et al.* 2010; Sander *et al.* 2011; Sander 2013; Barrett 2014; Benson *et al.* 2014). Whereas basally branching 'prosauropod' taxa appear to have remained relatively morphologically conservative (Barrett & Upchurch 2007; Young & Larvan 2010) the base of Sauropoda is associated with the appearance of numerous cranial traits hypothesized to have led to greater bite force, jaw processing power and increased robustness of the skull and mandible. These include the dorsoventral expansion of the mandibular symphysis, broadening of the snout, the development of 'lateral plates' of bone inferred to have braced the teeth, and gross changes to cranial shape (Upchurch & Barrett 2000; Barrett & Upchurch 2007; Upchurch *et al.* 2007). However, this hypothesized functional shift has not been tested quantitatively using biomechanical methods.

Button *et al.* (2014) employed finite element analysis (FEA) of the crania of *Diplodocus* and *Camarasaurus* to investigate ecological phenomena, and Lautenschlager *et al.* (2016) used similar methods to compare the mechanical performance of *Plateosaurus* with that of other herbivorous dinosaurs. Here, this methodology is extended to the mandible of *Camarasaurus*. In addition, the jaw adductor musculature of *Plateosaurus* and *Camarasaurus*, restored digitally from CT scan data, are described in a detailed, comparative context for the first time. *Plateosaurus* is similar in craniodental morphology to other 'prosauropods' whereas *Camarasaurus* exhibits the 'broad-crowned' craniodental morphology considered plesiomorphic for sauropods (e.g. Chure *et al.* 2010), so that comparison of these taxa provides an opportunity to test functional hypotheses associated with the purported functional and ecological shift at the base of Sauropoda. Two main hypotheses are tested here. Firstly, that calculated bite forces of *Camarasaurus* will exceed those of *Plateosaurus* as a result of the changes in craniomandibular shape and adductor chamber morphology seen in sauropods. Secondly, that the skull and mandible of *Camarasaurus* will mechanically outperform *Plateosaurus* when loaded to replicate a static bite, as measured by lower levels of both functionally-induced stress and total strain energy.

Institutional abbreviations. AMNH, American Museum of Natural History, New York City, USA; CMNH, Carnegie Museum of Natural History, Pittsburgh, USA; DINO, Dinosaur National Monument, Vernal, USA; MB.R, Museum für Naturkunde, Berlin, Germany.

MATERIAL AND METHOD

Virtual osteological reconstruction

CT scans of MB.R.1937, an adult individual of *Plateosaurus engelhardti* and CMNH 11338, a juvenile specimen of *Camarasaurus lentus*, were provided by Lawrence M. Witmer, with permission to use the *Plateosaurus* data from R. Goessling on behalf of the Humboldt Museum für Naturkunde. These scan data were imported into Avizo (v6.3.1, v7 and v8.0; Visualization Sciences Group; http://www.vsg3d.com). Complete reconstructions were made of *Camarasaurus* and *Plateosaurus* by assigning each cranial element of CMNH 11338 and MB.R.1937 to a separate label within the Avizo segmentation editor. Each specimen has suffered taphonomic deformation, with missing and warped elements. Retrodeformation was performed using translation, transformation and mirroring tools within Avizo (see Lautenschlager *et al.* 2014; Cuff & Rayfield 2015) to produce undistorted and complete 3D osteological reconstructions of *Camarasaurus* and *Plateosaurus*. See Button *et al.* (2016) for more information.

Virtual muscle reconstruction

Jaw adductor muscles were reconstructed from a combination of first-hand observations and examination of CT scans of MB.R.1937 and CMNH 11338. Muscle origination and insertion sites were identified on the basis of phylogenetic bracketing (Witmer 1995) and osteological correlates (see Holliday 2009), with topological constraints provided by other tissues and comparison to more distant outgroups (Lepidosauria (Fairman 1999; Holliday & Witmer 2007)) where appropriate. Additionally, comparisons were made with two earlier jaw muscle reconstructions of *Plateosaurus* (Galton 1985*b*; Fairman 1999). Virtual muscles were then constructed following the protocol of Lautenschlager (2013), with muscle size constrained by osteological and soft-tissue topological constraints.

Forces were calculated using the 'dry skull method' (Thomason 1991). Physiological cross-sectional area (PCSA) for each muscle was calculated by dividing the total volume of each muscle, measured using the Avizo material statistics module, by its estimated fibre length. As muscle pennation cannot be measured for extinct taxa, total muscle length, as measured from the midpoint of the

origination site to the midpoint of the attachment site, was taken as an approximation for fibre length, also measured in Avizo. In the absence of physiological data on sauropodomorph muscles this is necessary in order to minimize *ad hoc* assumptions; however, it should be noted that as muscle length represents the maximum possible fibre length it will produce a minimum estimate of muscle force. PCSA values were multiplied by the upper and lower values of the specific tension of muscle as reported by Thomason *et al.* (1990) (147–392 kPa) to produce upper and lower bounds of contractile muscle force.

CMNH 11338 represents a juvenile *Camarasaurus lentus*. The adductor musculature was first reconstructed on the juvenile-sized skull. Then, in order to provide an estimate of adult bite force, this juvenile skull model (with the reconstructed adductor muscles) was scaled up to reach the dimensions of adult *C. lentus* skulls. Differences in skull proportions between CMNH 11338 and adult *C. lentus* fall within the range of variation observed between adult specimens (Ikejiri *et al.* 2005). Indeed, no significant ontogenetic changes in skull morphology, beyond a general size increase, are currently recognized for *C. lentus* (Ikejiri *et al.* 2005). In this case, the digital model, with reconstructed muscle volumes, was scaled by 180% in all axes to match the linear dimensions of the adult individual DINO 28 (Madsen *et al.* 1995) as in Button *et al.* (2014). The force provided by each of these adult-scaled adductor muscles was then calculated following the same protocol as described above. It should be noted, however, that the low sample size of relatively complete skulls of *Camarasaurus* means that the relative influences of ontogenetic and individual variation are unknown. This is further complicated by the absence of species-level apomorphies in the crania of *Camarasaurus* spp. (Madsen *et al.* 1995; Ikejiri *et al.* 2005); a comprehensive review of referred cranial material is necessary to elucidate any other potential ontogenetic trends. As a result, the estimates of adult bite force presented herein should be treated with caution.

Bite force calculation

Resultant bite force will depend not only on muscle mass, but also on the line of muscle action and the mechanical efficiency of the mandible. To quantify these factors, the angle of each muscle line of action to the vertical was measured in both the sagittal (α) and coronal (β) planes. Additionally, the mechanical advantage (MA_{musc}; see Westneat 1994) was calculated for each muscle as the ratio between the inlever and outlever, measured at a gape angle of 12°. The inlever was measured as the length of a perpendicular line drawn between the line of muscle action and the jaw joint. The outlever was then measured

as the distance from the jaw joint to the biting tooth. MA_{musc} was calculated for bites at both the anteriormost and posteriormost dentary teeth, representing the minimum and maximum bite forces along the dentary tooth row, respectively. These measurements and the contractile force of each muscle (F_{musc}) permit the calculation of the force (F_{out}) supplied by each muscle at these bite positions through simple lever mechanics (e.g. Reichel 2010; Sakamoto 2010; Lautenschlager 2013):

$$F_{out} = (F_{musc} \times \cos(\alpha) \times \cos(\beta)) \times MA_{musc}$$

Total bilateral bite force was then calculated as the sum of these forces from each side of the skull for *Plateosaurus* and both the juvenile and adult-scaled models of *Camarasaurus*.

Finite element analysis

Finite element models. Osteological reconstructions of the skull and mandible were imported into HyperMesh (v11; Altair; http://www.altairhyperworks.co.uk/product/Hyper-Mesh) for meshing. Standard element clean-up procedures were conducted within HyperMesh yielding models with the following numbers of tetrahedral elements: *Plateosaurus* skull, 1 919 342; *Plateosaurus* mandible, 264 283; *Camarasaurus* skull, 877 796; and *Camarasaurus* mandible, 198 154. Bites were simulated at the anteriormost and posteriormost teeth of the cranium and the mandible and at a midpoint bite position. A summary of the models solved is given in Table 1.

Material properties. The material properties and anisotropy of tissues cannot be measured directly in extinct taxa, but have to be estimated from extant analogues. However, validation studies have demonstrated that FEA can accurately replicate patterns of stress and strain, if not the absolute magnitudes of these forces, even when approximated, isotropic properties are applied (Strait *et al.* 2005; Bright & Rayfield 2011; Bright 2014). Hence, meaningful comparisons can still be made between different models, provided that the material properties are consistent between them. Bovine Haversian bone was chosen as an analogue for sauropod cranial bone due to the histological similarity between it and sauropod long bones (Curry 1999; Sander *et al.* 2011); unfortunately, histological sections from sauropodomorph crania are currently lacking.

Bone properties assigned to the models were identical to those of bovine Haversian bone (Young's Modulus = 23.1 GPa, Poisson's ratio = 0.29; see Reilly & Burstein 1975). These measurements were reported from cattle femora, and so are likely to be overestimated with respect to the properties of cranial bone; as a result, the lowest value for the Poisson's ratio was chosen, as in previous analyses of sauropodomorph crania (Young *et al.* 2012;

TABLE 1. Description of the different models created for use in this analysis.

Model	Elements	Surface area (mm²)	Volume (mm³)	Total applied force (N)	Teeth constrained
Plateosaurus					
Cranium					
Anterior bite	1 919 342	153 845	294 690	607.04	Two anteriormost premaxillary teeth on each side
Mid bite	1 919 342	153 845	294 690	607.04	First two maxillary teeth on each side
Posterior bite	1 919 342	153 845	294 690	607.04	Two posteriormost maxillary teeth on each side
Mandible					
Anterior bite	264 283	66 172	99165.3	607.04	Two anteriormost dentary teeth on each side.
Mid bite	264 283	66 172	99165.3	607.04	Seventh and eighth dentary teeth on each side
Posterior bite	264 283	66 172	99165.3	607.04	Two posteriormost dentary teeth on each side
Unilateral anterior bite	264 283	66 172	99165.3	607.04	Two anteriormost teeth on the right side of the dentary
Unilateral mid bite	264 283	66 172	99165.3	607.04	Seventh and eighth dentary teeth on the right side
Unilateral posterior bite	264 283	66 172	99165.3	607.04	Two posteriormost dentary teeth on the right side
Plateosaurus 'structural comparison'					
Cranium					
Anterior bite	1 919 342	153 845	294 690	1062.26	Two anteriormost premaxillary teeth on each side
Mid bite	1 919 342	153 845	294 690	1062.26	First two maxillary teeth on each side
Posterior bite	1 919 342	153 845	294 690	1062.26	Two posteriormost maxillary teeth on each side
Mandible					
Anterior bite	264 283	66 172	99165.3	1353.7	Two anteriormost dentary teeth on each side
Mid bite	264 283	66 172	99165.3	1353.7	Seventh and eighth dentary teeth on each side
Posterior bite	264 283	66 172	99165.3	1353.7	Two posteriormost dentary teeth on each side
Unilateral anterior bite	264 283	66 172	99165.3	1353.7	Two anteriormost teeth on the right side of the dentary
Unilateral mid bite	264 283	66 172	99165.3	1353.7	Seventh and eighth dentary teeth on the right side
Unilateral posterior bite	264 283	66 172	99165.3	1353.7	Two posteriormost dentary teeth on the right side
Camarasaurus juvenile					
Cranium					
Anterior bite	877 796	266020.5	1 020 094	1836.8	Two anteriormost premaxillary teeth on each side
Mid bite	877 796	266020.5	1 020 094	1836.8	First two maxillary teeth on each side
Posterior bite	877 796	266020.5	1 020 094	1836.8	Two posteriormost maxillary teeth on each side
Mandible					
Anterior bite	198 154	89 787	400 838	1836.8	Two anteriormost teeth on each side
Mid bite	198 154	89 787	400 838	1836.8	Fifth and sixth dentary tooth constrained on each side
Posterior bite	198 154	89 787	400 838	1836.8	Two posteriormost dentary teeth on each side
Unilateral anterior bite	198 154	89 787	400 838	1836.8	Two anteriormost teeth on the right side of the dentary
Unilateral mid bite	198 154	89 787	400 838	1836.8	Fifth and sixth dentary teeth on the right side
Unilateral posterior bite	198 154	89 787	400 838	1836.8	Two posteriormost dentary teeth on the right side

In addition to the tooth constraints detailed here, all models were also constrained at the quadrates. Two sets of *Plateosaurus* cranium models were created: those scaled as per the life reconstruction and those scaled so that the ratio between cranium surface area and applied muscle force matched that reconstructed for *Camarasaurus* (the 'structural comparison'). Similarly, two mandible models were also created: those scaled as per the life reconstruction and a 'structural comparison' where those the ratio between mandible surface area and applied muscle force was scaled to match that of *Camarasaurus*. Bite forces were calculated for the minimum and maximum muscle forces as calculated for each taxon.

Button *et al.* 2014). Teeth were assigned the properties of vertebrate enamel (Young's Modulus = 80 GPa, Poisson's ratio = 0.3; see Ichim *et al.* 2007) and dentine (Young's Modulus = 21 GPa, Poisson's ratio = 0.31; see Gilmore *et al.* 1969). Difficulty with separating dentine and enamel led to teeth being assigned properties of a singular, intermediate tissue (Young's Modulus = 50.5 GPa, Poisson's ratio = 0.305), and no periodontal ligament was modelled. Some validation studies have suggested that these simplifications have minimal influence on the overall patterns of stress and strain recovered (Wood *et al.* 2011; Fitton *et al.* 2015; but see Gröning *et al.* 2011) and

comparisons between models where teeth were assigned properties of pure dentine or enamel show little difference between models using different values (see Button *et al.* 2016). In the absence of data on dinosaur cranial bone anisotropy, all materials were assumed to be isotropic to minimize *ad hoc* assumptions.

Model constraints. Artificially inflated stresses can be associated with point constraints (Bright 2014). To mitigate this, constraints were modelled as a series of rigid links (a 'diffuse coupling constraint' or DCC), spreading the constraint over a series of nodes (Young *et al.* 2012; Button *et al.* 2014).

All skull models were constrained against translation in the x (anteroposterior), y (dorsoventral) and z (mediolateral) planes at the quadrates. Mandible models were constrained against translation in all three of these axes at the articular glenoid. Each model was then constrained against translation in the y plane (the axis of biting) at the four biting teeth. The location of the biting teeth was varied in order to simulate bilateral bites at three different locations along the tooth row, as detailed in Table 1.

The mandibular symphysis is particularly important in the transferral of forces during asymmetric biting (Porro *et al.* 2011). To test the importance of the expansion of the symphysis in sauropods more thoroughly, unilateral anterior, midpoint and posterior bites were also modelled for the mandible with only the teeth on the right-hand side constrained (Table 1).

Model loading. Models were loaded with maximum adductor muscle forces as calculated above. Loads were applied across multiple nodes on the muscle origination/insertion sites of the skull and mandible, respectively. This was performed using a custom-built macro supplied by Altair, which simultaneously loads multiple nodes, projected towards a node resulting in a vector equivalent to the line of action of each muscle. Muscle forces applied to the adult *Camarasaurus* model were scaled up from those of the juvenile so that total applied force remained in the same proportion to surface area. As a consequence, results from finite element modelling of an adult skull are redundant with respect to the results derived from the juvenile model (Dumont *et al.* 2009) and so are not reported below.

Two separate load cases were applied to the *Plateosaurus* skull and mandible models. The first load case applied the estimated muscle forces for *Plateosaurus*, as calculated above. A second set of 'structural' analyses was performed in an effort to disentangle the effects of size and shape in the relative performance of crania. For these analyses the muscle forces applied to the *Plateosaurus* skull and mandible models were scaled so that the ratio between overall force and skull/mandible surface area, as measured in Avizo, was constant in both taxa. This accounts for the differences in size and relative adductor

muscle mass between them (Dumont *et al.* 2009), so that the resulting comparisons of stress and strain values primarily highlights differences in induced stress and strain due to cranial or mandibular shape.

Analyses. Models were exported to Abaqus (v6.10.2; Dassault Systèmes Simulia; http://www.3ds.com/products-services/simulia/products/abaqus/) for solving. Relative performance of each skull was gauged through comparison of functionally incurred von Mises stresses. Von Mises stress represents a single value of 'overall stress', approximating the proximity to failure of a tissue and so provides a measure of the strength of a structure under loading (Rayfield 2007; Dumont *et al.* 2009). Additionally, comparisons were made between the contour plots representing principal stresses and strains.

The mechanical efficiency of the skull and mandible of both taxa was compared by computing the total strain energy of each model under replicated bilateral biting. This metric represents the external energy spent deforming a body under loading; lower values hence describe structures which are more efficient at transmitting applied forces (Dumont *et al.* 2009).

The total strain energy was computed for the *Camarasaurus*, *Plateosaurus* and scaled *Plateosaurus* (see above) cranium and mandible models when performing a bilateral bite at the anterior, midpoint and posterior biting points. However, whereas stress varies with surface area, the total strain energy is proportional to the square of the total applied force and the cube of the volume of each model (Dumont *et al.* 2009). In order to correct for the differences in volume between the cranium and mandible of each taxon, the strain energy values obtained from the scaled *Plateosaurus* models were multiplied by (Volume$_{Plateosaurus\ model}$/ Volume$_{Camarasaurus\ model}$)$^{1/3}$, following Dumont *et al.* (2011). Comparison of the resulting strain energy value with those obtained from the *Camarasaurus* models allowed the relative efficiency of each structure to be judged in the context of the shape differences between them.

RESULTS

Muscle origination and insertion site reconstruction

The abbreviations for the jaw adductor muscles used herein are given in Table 2. Identified muscle origination and insertion sites are shown in Figure 1 and summarized in Table 3. The level of inference (*sensu* Witmer 1995, 1997) of each attachment site is indicated.

m. adductor externus superficialis (m.AMES). The origination and insertion areas of the m.AMES are highly

TABLE 2. Muscle abbreviations as used in this study.

Group	Muscle	Abbreviation
m. adductor mandibulae externus	m. adductor manidbulae externus superficialis	m.AMES
	m. adductor manidbulae externus medialis	m.AMEM
	m. adductor manidbulae externus profundus	m.AMEP
m. pseudotemporalis	m. pseudotemporalis superficialis	m.PSTs
	m.pseudotemporalis profundus	m.PSTp
	m. adductor mandibulae posterior	m.AMP
m. pterygoideus	m. pterygoideus dorsalis	m.PTd
	m. pterygoideus ventralis	m.PTv

conserved across sauropsids (Holliday & Witmer 2007; Holliday 2009). These origination and insertion sites can be identified by the smooth scars they leave on the temporal bar and the surangular, respectively, even if more specific osteological correlates are rare (Holliday 2009). As a result, both of the attachment areas of the m.AMES can be reconstructed as robust level I inferences.

In both *Plateosaurus* and *Camarasaurus* the m.AMES is reconstructed as originating from the smooth dorsomedial and medial surfaces of the postorbital posterior process and the medial surface of the squamosal anterolateral process. This smooth surface extends posteriorly onto the main body of the squamosal in both taxa, indicating that the m.AMES extended into the posterior corner of the supratemporal fenestra. Anteriorly, the origination area of the m.AMES is bounded by that of the m.PSTs.

The m.AMES is then reconstructed as inserting onto an elongate smooth region on the dorsolateral edge of the surangular. This surface is strongly bevelled in *Plateosaurus* and more modestly so in *Camarasaurus*. The mediolateral thickness of the m.AMES is well constrained by its topological relationships with the other muscles of the m.AME group. The origination and insertion sites of the muscle as reconstructed here are identical to those of Galton (1985*b*) and Fairman (1999).

m. adductor mandibulae externus profundus (m.AMEP). The origination and insertion sites of the m.AMEP are also conserved across sauropsids (Holliday & Witmer 2007) and so can be reconstructed with confidence in sauropodomorphs (Holliday 2009). However, as the m.AMEP and m.AMEM can be difficult to distinguish from each other, there can be some ambiguity in interpreting the osteological correlates left by these muscles (Holliday & Witmer 2007; Holliday 2009).

The m.AMEP fills the anteromedial region of the supratemporal fenestra in sauropsids, attaching to the lateral surface of the parietal (Holliday & Witmer 2007; Holliday 2009). In *Plateosaurus* it primarily attaches to the main body of the parietal. In *Camarasaurus*, however, the anteroposterior shortening of the parietal means that the m.AMEP primarily originates on the medial portion of the posterolateral wing of the parietal, with the m.AMEM then occupying the more posterolateral portion. The boundary between the origination areas of the m.AMEP and m.AMEM is marked by a small scar (more obvious in *Camarasaurus*) in both taxa (Holliday 2009). Anteriorly, the m.AMEP is bounded by the m.PSTs. As a result, the origination area of the m.AMEP can be reconstructed as a level I inference in *Plateosaurus* and *Camarasaurus*.

The m.AMEP inserts onto the coronoid eminence in all sauropsids (Holliday & Witmer 2007; Holliday 2009) and is hence a level I inference in sauropodomorphs (Holliday 2009). It is here reconstructed as attaching to the dorsomedial surface of posterior end of the coronoid and the anterior end of the surangular in both taxa. The attachment region on the dorsomedial surface of the surangular is narrow (especially so in *Plateosaurus*), smooth and slightly concave. The posterior extent of the m.AMEP is difficult to constrain as it is continuous with the m.AMEM. In *Plateosaurus* a weak break is observed between the two elongate, slightly concave scars observed on the dorsomedial edge of the surangular. In *Camarasaurus* this break is more pronounced, separating a circular, slightly dorsoventrally expanded scar at the anterior end of the surangular from a more elongate one running posteriorly. This break is here taken as indicating the boundary between the insertion sites of the m.AMEP and

FIG. 1. Reconstructed jaw adductor origination and insertion sites. A–F, jaw adductor muscle origination and insertion sites identified in *Plateosaurus engelhardti*; the potential for a more expansive origination of the m.PTd (see text) is indicated by m.PTd (alt); A, skull in left lateral view; the illustrated distribution of the m.AMES refers to the insertion area on the medial surface of the postorbital bar; B, left half of the cranium in left lateral view, with the jugal, quadratojugal, postorbital and lacrimal removed to reveal the epipterygoid and palate; C, cranium in ventral view; D, cranium in dorsolateral view; E, right mandible in medial view; F, right mandible in dorsolateral view. G–L, jaw adductor muscle origination and insertion sites in *Camarasaurus lentus*; G, skull in right lateral view; the illustrated distribution of the m.AMES refers to the insertion area on the medial surface of the postorbital bar; H, cranium in right lateral view with the postorbital and jugal removed, revealing the palate; I, cranium in ventral view; J, cranium in dorsal view; K, right mandible in medial view; L, right mandible in dorsolateral view. All scale bars represent 100 mm. For muscle abbreviations, see Table 2.
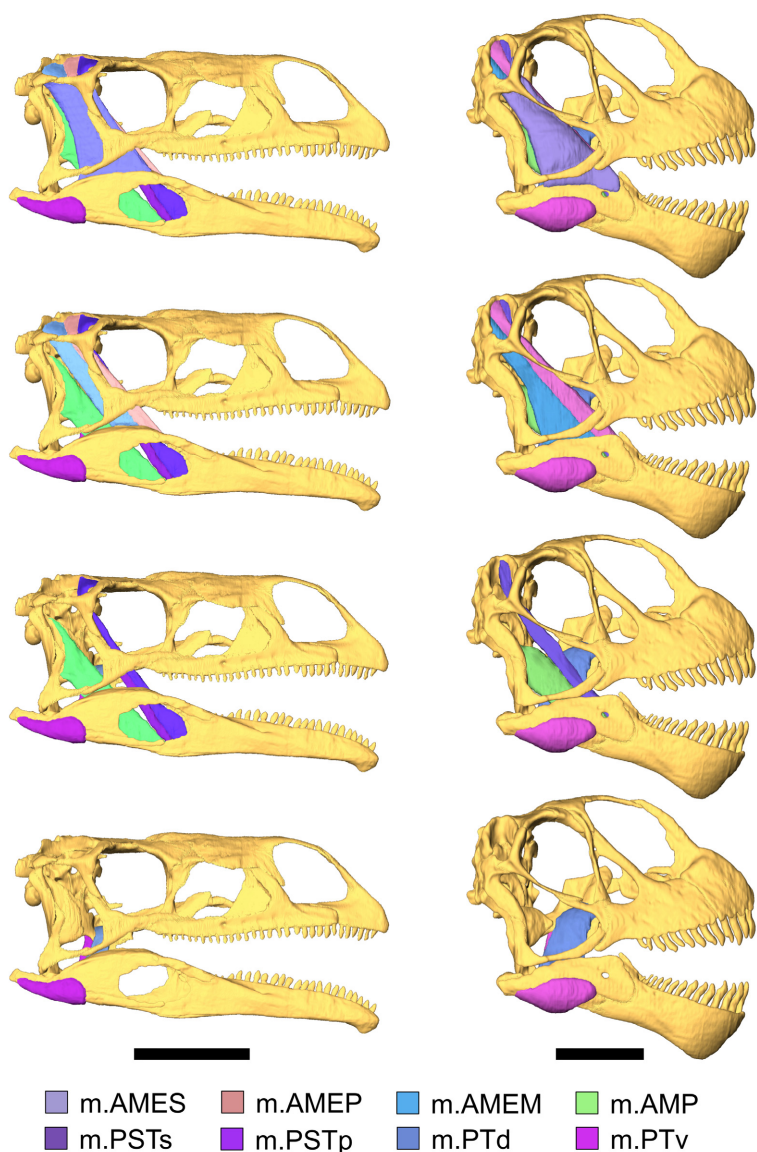
m.AMES m.AMEP m.AMEM m.AMP
m.PSTs m.PSTp m.PTd m.PTd (alt) m.PTv
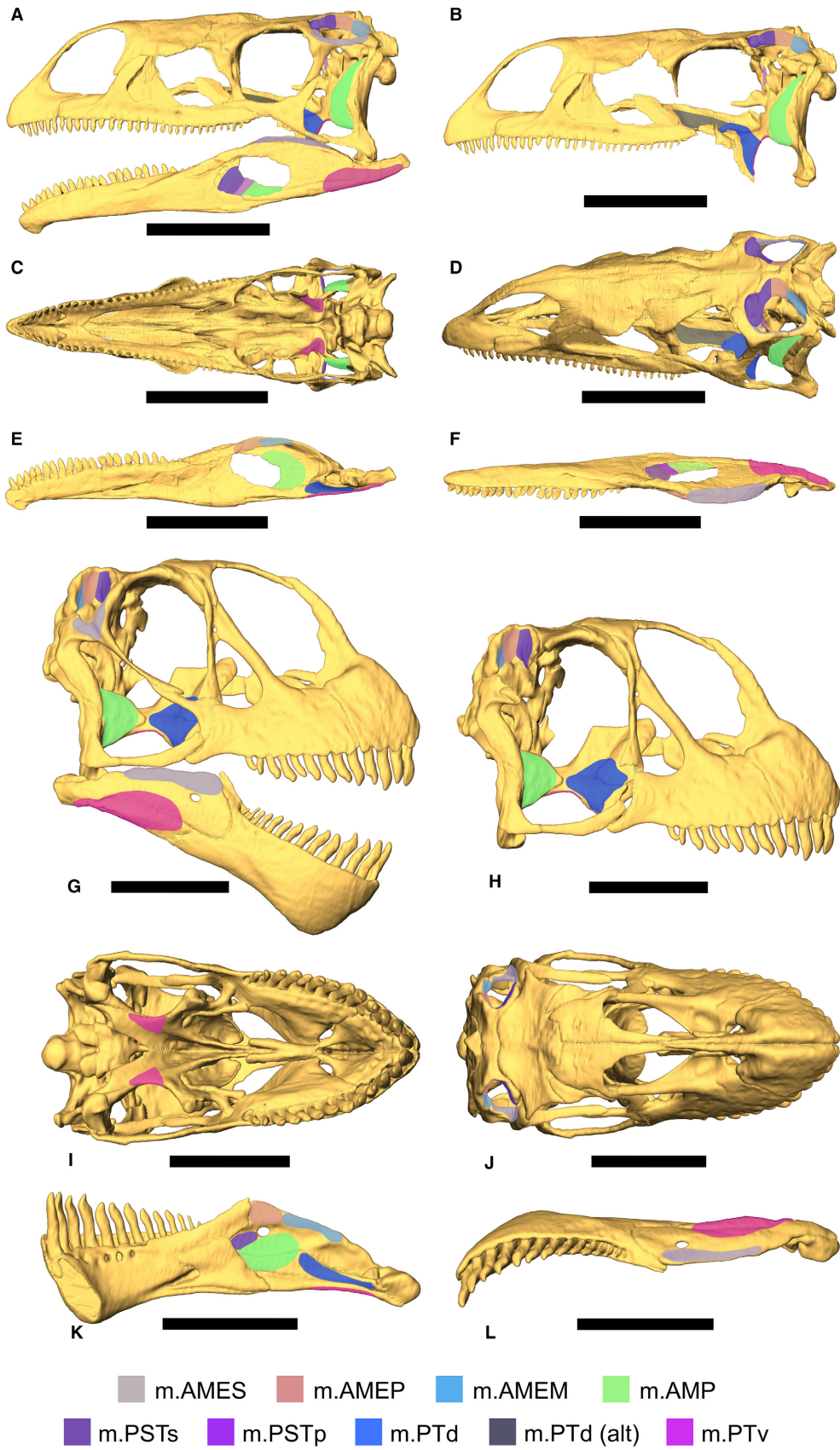
FIG. 2. Reconstructed jaw adductor musculature for *Plateosaurus* (left) and *Camarasaurus* (right), in right lateral view. Reconstructions are shown at multiple depths, with the removal of successively superficial muscles groups. From top to bottom: all muscles; removal of the m.AMES, removal of the m.AME group, removal of the m.AME, m.PST and m.AMP groups. Scale bars represent 100 mm.

☐ m.AMES	☐ m.AMEP
☐ m.PSTs	☐ m.PSTp

m.AMEM ☐ m.AMP ☐
m.PTd ☐ m.PTv ☐

the m.AMEM, with the m.AMEP inserting anterior to it in both taxa. The anterior extent of the m.AMEP, as well as its size and orientation, is further constrained in *Plateosaurus* by the position of the ectopterygoid. The ectopterygoid of *Camarasaurus* is positioned more anteriorly, relieving these constraints. The origination and insertion sites of the muscle as reconstructed here are identical to those of Fairman (1999) and Galton (1985*b*).

m. adductor externus medialis (m.AMEM). The origination site of the m.AMEM is also conserved across archosaurs, where it occupies the posterior region of the supratemporal fenestra (Holliday & Witmer 2007; Holliday 2009). It attaches to the posterolateral wing of the parietal (Holliday & Witmer 2007; Holliday 2009) occupying a large, smooth region evident in both *Plateosaurus*

and *Camarasaurus*. The anteromedial boundary of the m.AMEM is constrained by the position of the m.AMEP, as described above. As a result, the origination area of the m.AMEM can be reconstructed as a level I inference in both taxa.

The m.AME inserts onto a narrow, slightly concave, region along the dorsomedial edge of the surangular, posterior to the m.AMEP, in sauropodomorphs (Holliday 2009). Distinguishing the insertions of these two muscles can be problematic; the m.AMEM is here considered to occupy the posterior of the two partially distinct scars in this region, as described above. This attachment runs posteriorly to the point where the dorsomedial edge of the surangular pinches out. Nevertheless, the distinction made between the insertion sites of these muscles here is somewhat ambiguous, particularly as the insertion of the
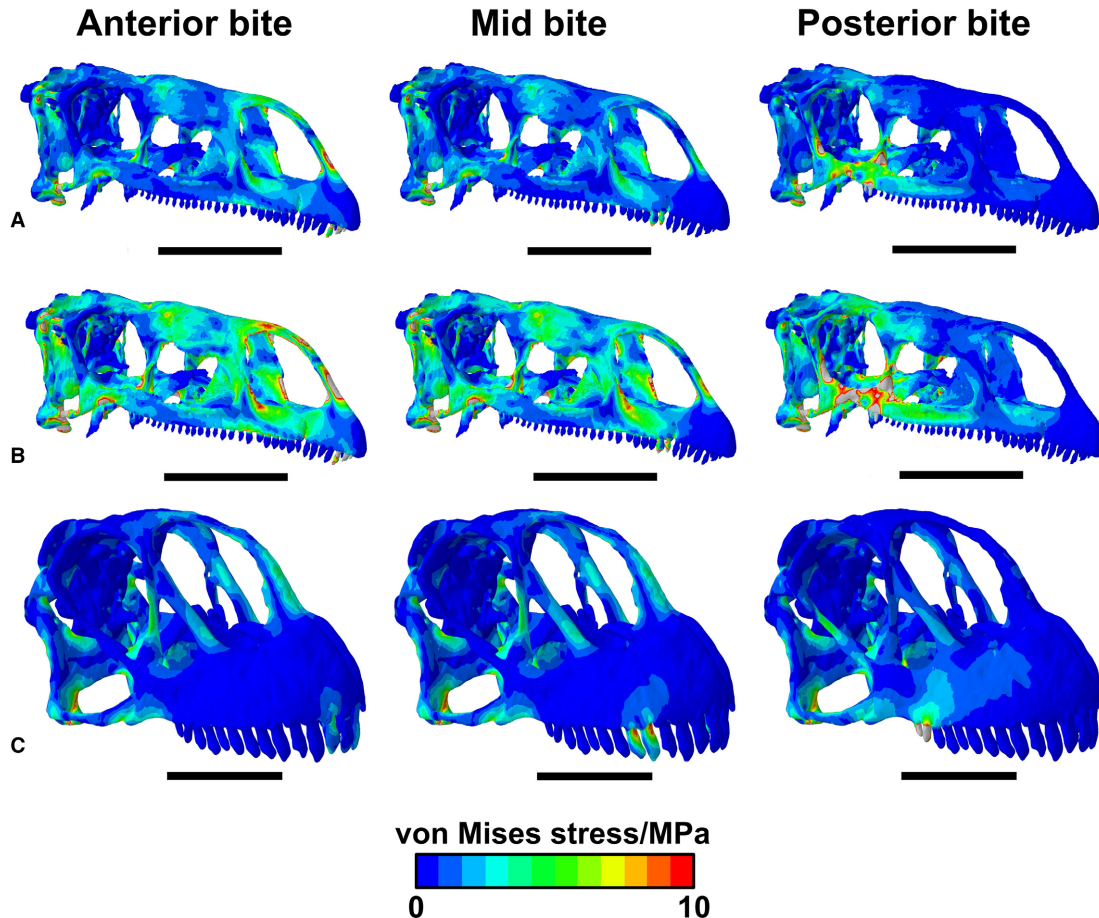
FIG. 3. Von Mises stress contour plots from FEA of the crania of *Plateosaurus* and *Camarasaurus* for anterior (left), midpoint (middle) and posterior (right) bites, in oblique lateral view. A, results for the unscaled *Plateosaurus* model. B, results for *Plateosaurus* when scaled so that the ratio of applied muscle force:skull surface area equals that of *Camarasaurus*, for the 'structural comparison'. C, results for *Camarasaurus*. Scale bars represent 100 mm.

m.AMEM lacks a specific, distinct correlate in extant crocodilians and birds (Holliday 2009). As a result, the insertion of the m.AMEM reconstructed here represents a level I′ inference. The origination and insertion sites of the muscle as reconstructed here are identical to those of Fairman (1999) and Galton (1985*b*).

m. pseudotemporalis superficialis (m.PSTs). The m.PSTs is the deepest and most anteriorly positioned of the temporal muscles. In archosaurs it originates from the anterior wall of the supratemporal fenestra (Holliday & Witmer 2007; Holliday 2009). This allows the origination area of the m.PSTs to be reconstructed as a level I inference in sauropodomorphs, although the generally smooth surface of the supratemporal fossa means that it can be difficult to distinguish this attachment from those of the m.AMEP and m.AMES. In both taxa the m.PSTs is reconstructed as occupying most of the anterolateral wing of the parietal and the posterior wall of the

laterosphenoid. In *Plateosaurus* the m.PSTs also originates from the frontal, whereas the frontal is excluded from the supratemporal fossa in neosauropods such as *Camarasaurus* (Upchurch *et al.* 2004). In *Plateosaurus* the supratemporal fossa is deeply incised into the frontal. This is preserved on both sides of the skull of MB.R. 1937 as well as in other *Plateosaurus* skulls (e.g. AMNH FARB 6810; Prieto-Márquez & Norell 2011). Consequently, it does not appear to represent a taphonomic artefact. A similar 'ovoid fossa' is known in various other basal sauropodomorph taxa, including *Unaysaurus*, *Jingshanosaurus* and *Melanorosaurus* (Yates 2007). Deep fossae are also observed on the frontals of some ornithischians (e.g. Sereno & Dong 1992) and also in theropods, where they have been reconstructed as representing part of the origination area of the m.PSTs (Coria & Currie 2002; Molnar 2008) although the strong horizontal orientation of the fossa makes this somewhat problematic (Holliday 2009). In *Plateosaurus*, however, it is

TABLE 3. Summary of origination and insertion sites for each muscle in *Plateosaurus* and *Camarasaurus* as reconstructed for this study.

Muscle	Origin	Level of inference	Insertion	Level of inference
Plateosaurus				
m.AMES	Lateral portion of the supratemporal fossa; medial surface of the upper temporal bar	I	Lateral surface of the dorsal edge of the surangular	I
m.AMEP	Posteromedial portion of supratemporal fossa; lateral surface of the parietal	I	Medial surface of the coronoid region; posterior portion of the medial edge of the coronoid and anterior portion of the dorsomedial edge of the surangular	I
m.AMEM	Posterior portion of the supratemporal fossa; anterior face of the posterolateral wing of the parietal and the medial process of the squamosal	I	Dorsomedial edge of the surangular	I′
m.PSTs	Anterior portion of the supratemporal fossa; posterior edge of the frontal and posterior surface of the parietal anterolateral wing	I	Anterior portion of the mandibular adductor fossa	II′
m.PSTp	Dorsolateral surface of the epipterygoid	I	Anteroventral portion of the mandibular adductor fossa	III′
m.AMP	Lateral surface of the pterygoid wing of the quadrate	I	Mandibular adductor fossa	I
m.PTd	Dorsal surface of the pterygoid	I	Medial surface of prearticular and articular	I
m.PTv	Posteroventral surface of the pterygoid	I	Ventral surface of angular and prearticular; wraps onto the lateral surface of the mandible	I
Camarasaurus				
m.AMES	Lateral portion of the supratemporal fossa; medial surface of the upper temporal bar	I	Lateral surface of the dorsal edge of the surangular	I
m.AMEP	Posteromedial portion of supratemporal fossa, lateral surface of the parietal	I	Medial surface of the coronoid region and anterior portion of the dorsomedial edge of the surangular	I
m.AMEM	Posterior portion of the supratemporal fossa; anterior face of the distal portion of the parietal posterolateral wing and the medial process of the squamosal	I	Dorsomedial edge of the surangular	I′
m.PSTs	Anterior portion of the supratemporal fossa; posterior surface of the parietal anterolateral wing	I	Anterior portion of the mandibular adductor fossa	II′
m.PSTp	Muscle absent?		Muscle absent?	
m.AMP	Lateral surface of the pterygoid wing of the quadrate	I	Mandibular adductor fossa	I
m.PTd	Dorsal surface of the pterygoid	I	Medial surface of prearticular and articular	I
m.PTv	Posteroventral surface of the pterygoid	I	Ventral surface of angular and prearticular; wraps onto the lateral surface of the mandible	I

Levels of inference (*sensu* Witmer 1995) are given for each. See Table 2 for muscle abbreviations.

oriented posterodorsally. This, coupled with the continuity between this depression and the rest of the supratemporal fossa, means that it is reconstructed here as forming part of the origination area of the m.PSTs. This is consistent with previous reconstructions of the m.PSTs in *Plateosaurus* (Galton 1985*b*; Fairman 1999).

Reconstruction of the insertion site of the m.PSTs in sauropodomorphs is problematic. Haas (1963), Galton (1985*b*) and Fairman (1999) reconstructed the m.PSTs as inserting onto the medial surface of the coronoid, as in extant lepidosaurs. However, phylogenetic bracketing (Holliday 2009) suggests that an anterior insertion within the mandibular fossa, as in extant crocodiles and most

ratites (Holliday & Witmer 2007; Holliday 2009) is more likely. Further evidence of this comes from topological constraints. An insertion onto the coronoid would also result in problems in the spatial relationships of the m.PSTs with the other adductor muscles in both taxa. This is particularly marked in *Plateosaurus*, where the coronoid eminence is small relative to the mandibular fossa and the adductor chamber is very narrow. The adductor fossa in *Camarasaurus* differs from the plesiomorphic condition seen in *Plateosaurus* and crocodilians as it exhibits closure of the external mandibular fenestra. However, there is no reason to assume this was accompanied by relocation of the attachment site for the m.PSTs. The m.PSTs is hence reconstructed as inserting into the anterior region of the mandibular fossa in both *Plateosaurus* and *Camarasaurus* on the basis of phylogenetic bracketing and topological constraints. However, the absence of a specific osteological correlate for this attachment and its variability among extant birds (Holliday & Witmer 2007; Holliday 2009) render this a level II′ inference.

The mediolateral thickness of the m.PSTs is well constrained by the other adductor muscles and the palatal bones. This is particularly obvious in *Plateosaurus*, whose strongly developed pterygoid flange tightly constricts the thickness of the m.PSTs. The mandibular adductor fossa of *Plateosaurus* is also strongly laterally compressed, suggesting a tendinous (rather than fleshy) attachment of this muscle (Lautenschlager 2013) as in extant crocodilians (Holliday & Witmer 2007; Holliday 2009; Tsai & Holliday 2011; Holliday *et al.* 2013).

m. pseudotemporalis profundus (m.PSTp). Osteological correlates of m.PSTp attachment are rare, but phylogenetic bracketing indicates that origination on the anterolateral surface of the epipterygoid would have been plesiomorphic for dinosaurs (Holliday 2009). The m.PSTp is hence reconstructed as originating from the expanded anterolateral surface of the epipterygoid, dorsal to the midshaft in *Plateosaurus*, as a level I inference. By contrast, the epipterygoid was lost in neosauropods and it is possible that neosauropods lost the m.PSTp as a corollary (Holliday 2009). Consequently, this muscle was not reconstructed for *Camarasaurus*.

Reconstructing the mandibular insertion of the m.PSTp is highly problematic in sauropodomorphs as the muscle is typically vestigial in extant archosaurs and does not leave unambiguous osteological correlates (Holliday 2009). Fairman (1999) reconstructed the m.PSTp of *Plateosaurus* as attaching to the medial surface of the coronoid region, as in lepidosaurs and most birds (Holliday & Witmer, 2007; Holliday, 2009). However, the small area available for attachment on the mediodorsal edge of the surangular, and topological constraints provided by other muscles (particularly the m.PSTs), suggest that such an insertion is unlikely in *Plateosaurus*. Instead, the m.PSTp is reconstructed as attaching within the mandibular adductor fossa adjacent to the m.PSTs, similar to the condition observed in crocodilians (Holliday & Witmer 2007; Holliday 2009) and as reconstructed for the theropod *Erlikosaurus* (Lautenschlager 2013). Still, it should be noted that in extant crocodilians the m.PSTp merges into the m.PTd rather than directly inserting onto the mandible itself (Holliday & Witmer 2007; Holliday *et al.* 2013). The absence of a specific osteological correlate and variation within the extant phylogenetic bracket for this character render its reconstruction a level III′ inference; the lowest confidence associated with any of the reconstructed attachment sites discussed herein.

m. adductor mandibulae posterior (m.AMP). The insertion and origination sites for the m.AMP are highly conserved across all sauropsids (Holliday & Witmer 2007; Holliday 2009) allowing them to be reconstructed in sauropodomorphs as robust level I inferences. The m.AMP would have attached to the wide surface provided by the expansive pterygoid wing of the quadrate in both *Plateosaurus* and *Camarasaurus*, as in other dinosaur taxa including *Diplodocus* (Holliday 2009; Young *et al.* 2012; Button *et al.* 2014).

The m.AMP would have inserted into the mandibular fossa in both taxa, as in other dinosaurs (Holliday 2009). Galton (1985*b*) and Fairman (1999) reconstructed the m.AMP as filling the entire mandibular fossa in *Plateosaurus*. However, the insertions of the m.PSTs and m.PSTp in the mandibular fossa, as reconstructed here, restricts that of the m.AMP to the posterior two-thirds of the fossa in both taxa. In *Camarasaurus*, the generally smooth surface of the fossa extends from the surangular onto the medial surface of the prearticular, suggesting that the m.AMP insertion extended ventrally to cover some of the prearticular also.

m. pterygoideus dorsalis (m.PTd). Origination and insertion sites of the m.PTd are highly conserved across sauropsids, allowing robust level I inferences of attachment sites in sauropodomorphs (Holliday & Witmer 2007; Holliday 2009). In *Camarasaurus*, the shortened pterygoid and anterior position of the ectopterygoid allow the m.PTd to be reliably reconstructed as originating from the dorsal surface of the pterygoid and palatine, as its presence is recorded by a slightly depressed area, with a small crest on the palatine marking the probable anterior border of the attachment (see also Holliday 2009). In *Plateosaurus*, the m.PTd would have originated from the generally smooth lateral surface of the pterygoid flange and the dorsal surface of the pterygoid (Galton 1985*b*;

Fairman 1999). However, the anterior extent of this attachment is difficult to constrain, as its osteological correlates are poorly differentiated from those for the nasal passages and paranasal sinuses (Witmer 1997; Holliday 2009; Lautenschlager 2013). It extended at least as far anteriorly as the suture with the ectopterygoid, occupying a trough-like depression in the dorsolateral surface of the pterygoid, similar to the extent reconstructed for *Erlikosaurus* (Lautenschlager 2013), but no other features clarify whether (or how far) it extended further anteriorly. To quantify the impact of uncertainty in the anterior extent of this attachment on reconstructed muscle mass, a maximum estimate of the origination area was made in addition to this minimum estimate. In the maximum estimate, the m.PTd occupies the entire dorsolateral surface of the pterygoid ramus as far anteriorly as the suture with the palatine, as reconstructed for some theropods (e.g. Holliday 2009); the generally smooth and slightly concave morphology of this region offers some support for this reconstruction. Nevertheless, the extent of this attachment area has little impact on the cross-sectional area of the muscle, which is constrained by the surrounding soft and hard tissues within the adductor chamber, so the effect of this uncertainty on calculated muscle forces is minimal (Table 4).

The mandibular insertion site of the m.PTd is also a type I inference in sauropodomorphs (Holliday 2009). In both taxa the m.PTd attached to the medioventral surface of the prearticular, extending posteriorly to occupy a slight depression in the medial surface of the articular.

m. pterygoideus ventralis (m.PTv). The origination of the m.PTv, from the ventrolateral surface of the pterygoid, is highly conserved across sauropsids and can be reconstructed as a type I inference in sauropodomorphs (Holliday 2009), even if unambiguous correlates for the extent of this attachment are rare. The m.PTv is reconstructed in both taxa as originating from a smooth edge on the ventrolateral surface of the pterygoid, extending onto the ventral aspect of the pterygoid flange (Galton 1985*b*; Fairman 1999).

The insertion site of the m.PTv is also a class I inference in sauropodomorphs (Holliday 2009). It inserted onto the ventral edge of the angular and articular, wrapping around the ventral surface of the mandible to extend into an excavated area on its lateral surface (which is shallow in *Plateosaurus*, but prominent in *Camarasaurus*).

The thickness of the m.PTv is less well constrained. There are no osteological or reconstructed topological constraints on how far the main body of the muscle could have bulged medially towards the oral cavity. However, the lateromedial thickness of the dorsal end

of the m.PTv is indicated by the scar on the ventral surface of the pterygoid. As a result, to provide a conservative estimate, the muscle was then projected to maintain this thickness for the majority of its length.

Muscle volumetric reconstructions and forces

Calculated volumes, physiological cross-sectional areas and contractile forces are given in Table 4. The reconstructed volumes for each muscle are illustrated in Figure 2. Calculated muscle volumes and forces are lower in *Plateosaurus* than *Camarasaurus*, even after accounting for skull size (Table 4). These taxa also differ in the relative contributions provided by the different muscle groups to total bite force; a greater proportion of total bite force is provided by the palatal musculature (in particular the m.PTd) in *Camarasaurus*.

Uncertainty in the anterior extent of the m.PTd origin results in only a minor (*c.* 2.4%) difference in contractile muscle force, as the cross-sectional area of the main body of the m.PTd is tightly constrained by surrounding hard and soft tissues (Figs 1–2). Although the reconstruction of a more expansive origination of the m.PTd (Fig. 1A, B, D) does lead to an increase in overall muscle mass, the resulting increase in muscle length, used as a proxy for fibre length herein, leads to a lower calculated estimate of contractile force (Table 4). This discrepancy results from the way in which muscle forces were calculated. The relationship between muscle fibre and total length is not constant (e.g. van Eijden *et al.* 1997); total length only provides a maximum possible estimate of fibre length. Consequently, using total length as a proxy tends to underestimate contractile force; this effect may be particularly notable for more elongate muscles.

Calculated bite forces

Measured muscle angles, mechanical advantage for each muscle belly for both anterior and posterior bites and calculated bite forces are given in Table 5. Calculated bite forces for adult *Camarasaurus* greatly exceed those of both *Plateosaurus* and juvenile *Camarasaurus*. Reconstructed bite forces for the juvenile *Camarasaurus* also exceed those of *Plateosaurus*, even though their skulls are of similar length. Calculated anterior and posterior bite forces for the juvenile *Camarasaurus* are 329% and 325% those of *Plateosaurus*, respectively. Bite force as a proportion of total applied force is also greater for *Camarasaurus* than *Plateosaurus*, especially for anterior bites.

TABLE 4. Summary of adductor muscle volumes and calculated physiological cross-sectional areas (PCSA) for *Plateosaurus*, juvenile *Camarasaurus* and an adult *Camarasaurus*.

	Muscle volume (m^3)	PCSA (m^2) (Muscle volume/muscle length)	Minimum muscle force (N) (for 147 kPa)*	Maximum muscle force (N) (for 392 kPa)*
Plateosaurus engelhardti				
m.AMES	2.24×10^{-05}	2.47×10^{-04}	36.35	96.93
m.AMEP	6.76×10^{-06}	4.85×10^{-05}	7.13	19.02
m.AMEM	1.09×10^{-05}	9.31×10^{-05}	13.69	36.50
m.PSTs	6.89×10^{-06}	3.95×10^{-05}	5.81	15.49
m.PSTp	2.62×10^{-06}	1.87×10^{-05}	2.74	7.32
m.AMP	1.47×10^{-05}	1.40×10^{-04}	20.53	54.76
m.PTd	5.35×10^{-06}	8.30×10^{-05}	12.19	32.52
m.PTd (alt)	8.84×10^{-06}	6.47×10^{-05}	9.52	25.37
m.PTv	9.64×10^{-06}	1.05×10^{-04}	15.37	40.98
Total/Total (m.PTd (alt))	$1.58 \times 10^{-04}/1.65 \times 10^{-04}$	$1.55 \times 10^{-03}/1.51 \times 10^{-04}$	227.62/222.28	607.04/592.74
Total muscle PCSA/Cranium surface area		$1.01 \times 10^{-02}/9.82 \times 10^{-03}$		
Camarasaurus lentus juvenile				
m.AMES	6.93×10^{-05}	4.66×10^{-04}	68.4	182.3
m.AMEP	3.51×10^{-05}	1.79×10^{-04}	26.3	70.2
m.AMEM	3.83×10^{-05}	2.46×10^{-04}	36.2	96.4
m.PSTs	2.51×10^{-05}	1.22×10^{-04}	17.93	47.8
m.AMP	4.33×10^{-05}	3.89×10^{-04}	57.13	152.5
m.PTd	4.73×10^{-05}	4.82×10^{-04}	70.85	188.9
m.PTv	6.51×10^{-05}	4.60×10^{-04}	67.62	180.3
Total	6.48×10^{-04}	4.68×10^{-03}	688.86	1836.8
Total muscle PCSA/Cranium surface area		1.76×10^{-02}		
Camarasaurus lentus adult				
m.AMES	2.25×10^{-04}	1.51×10^{-03}	222.0	592
m.AMEP	1.14×10^{-04}	5.8×10^{-04}	85.26	227.4
m.AMEM	1.24×10^{-04}	7.97×10^{-04}	117.2	312.4
m.PSTs	8.13×10^{-05}	3.95×10^{-04}	58.07	154.8
m.AMP	1.40×10^{-04}	1.26×10^{-03}	185.2	493.9
m.PTd	1.53×10^{-04}	1.56×10^{-03}	229.3	611.5
m.PTv	2.11×10^{-04}	1.49×10^{-03}	219.0	584.1
Total	1.05×10^{-03}	7.59×10^{-03}	2232.06	5952.2
Total muscle PCSA/Cranium surface area		1.76×10^{-02}		

Values given are those calculated for each individual muscle on each side of the skull, so that total PCSA and applied force across both sides of the skull are double the sum of the individual values given here. For *Plateosaurus* values for both potential reconstructions of the m.PTd (one with the insertion area on the pterygoid being limited anteriorly and the other being more expansive; see text) are given. The ratio of total PCSA of all muscles (from both sides): the total cranium surface area is given to provide a value for total contractile muscle force corrected for differences in the size of the skull for each taxon.
*Upper and lower values of specific tension of muscle from Thomason *et al.* (1990).

Although there is uncertainty involved in the reconstruction of some muscles, a threefold difference in total muscle volume in either taxon is not tenable. The lower mechanical advantage means that the m.PTv, whose volume is poorly constrained, would need to be increased by over seven times its current size to provide the same output on bite force as that of *Camarasaurus*; such an enlargement cannot be accommodated. The relative biting performance of these taxa is hence robust to uncertainty in reconstructed adductor muscle volume.

Finite element analysis results

Von Mises stress values are given in Table 6, contour plots are given in Figures 3 and 4, and additional results, including principal stress and strain plots, are provided in Button *et al.* (2016). Both taxa exhibit broadly similar overall patterns and magnitudes of induced von Mises stress in the skull for all biting positions (cf. Fig. 3A, C), although observed stresses are slightly lower for *Camarasaurus* (Table 6). When corrected for differences in size

TABLE 5. Measurements taken to calculate anterior and posterior bite forces of *Plateosaurus engelhardti* and both juvenile and adult *Camarasaurus lentus*.

	Min F_{musc}	Max F_{musc}	α	β	aMA	pMA	Anterior bite		Posterior bite	
							Min force	Max force	Min force	Max force
Plateosaurus engelhardti										
m.AMES	36.35	96.93	23.7	1.95	0.206	0.402	6.85	18.27	13.37	35.66
m.AMEP	7.13	19.02	36.9	4.45	0.278	0.541	1.58	4.22	3.08	8.20
m.AMEM	13.69	36.5	32.6	2.95	0.233	0.455	2.68	7.16	5.24	13.97
m.PSTs	5.81	15.49	31.8	4.57	0.315	0.616	1.55	4.13	3.03	8.08
m.PSTp	2.74	7.32	31	4.92	0.258	0.505	0.60	1.61	1.18	3.16
m.AMP	20.53	54.76	34.3	1.03	0.163	0.318	2.76	7.37	5.39	14.38
m.PTd	9.52	32.52	31.6	21.9	0.106	0.207	0.80	2.72	1.56	5.32
m.PTv	15.37	40.98	43.5	20.8	0.097	0.189	1.01	2.70	1.97	5.25
Bite force							35.66	96.36	69.64	188.04
Bite force/total applied force							0.159	0.159	0.310	0.310
Camarasaurus lentus (juvenile)										
m.AMES	68.4	182.3	24.6	2.7	0.248	0.474	15.14	41.06	29.45	78.48
m.AMEP	26.3	70.2	31	7.41	0.350	0.669	7.82	20.88	14.96	39.92
m.AMEM	36.2	96.4	22.9	5.26	0.212	0.404	7.04	18.75	13.42	35.73
m.PSTs	17.93	47.8	27.1	8.64	0.334	0.638	5.27	14.05	10.07	26.84
m.AMP	57.13	152.5	35.5	9.01	0.199	0.380	9.14	24.40	17.46	46.60
m.PTd	70.85	188.9	25.6	21.2	0.123	0.234	7.33	19.54	13.94	37.17
m.PTv	67.62	180.3	16.2	18.3	0.129	0.246	7.95	21.21	15.17	40.44
Bite force							119.38	319.78	228.94	610.36
Bite force/total applied force							0.174	0.174	0.332	0.332
Camarasaurus lentus (adult)										
m.AMES	222	592	24.6	2.7	0.248	0.474	50.00	133.34	95.57	254.86
m.AMEP	85.26	227.4	31	7.41	0.350	0.669	25.37	67.65	48.48	129.31
m.AMEM	117.2	312.4	22.9	5.26	0.212	0.404	22.79	60.75	43.43	115.77
m.PSTs	58.07	154.8	27.1	8.64	0.334	0.638	17.07	45.50	32.61	86.92
m.AMP	185.2	493.9	35.5	9.01	0.199	0.380	29.63	79.03	56.59	150.91
m.PTd	229.3	611.5	25.6	21.2	0.123	0.234	23.71	63.24	45.11	120.31
m.PTv	219	584.1	16.2	18.3	0.129	0.246	25.76	68.70	49.12	131.00
Bite force							388.66	1036.42	741.82	1978.16
Bite force/total applied force							0.174	0.174	0.332	0.332

Minimum and maximum F_{musc} values refer to the contractile forces calculated in Table 4. α, angle of the muscle line of action from the vertical as measured in the sagittal plane; β, angle from the vertical in the coronal plane; aMA, mechanical advantage of each muscle for an anterior biting position; pMA, mechanical advantage for a posterior bite. Calculated contributions of each muscle and the total bilateral bite force are given.

and applied force (the 'structural comparison') differences in stress and strain accommodation are more apparent. Greater stress magnitudes are recorded for *Plateosaurus* in all biting positions (cf. Fig. 3B, C), with mean elemental stresses being 25–336% those of *Camarasaurus*, although the distribution of peak stresses and strains remain similar between the two taxa. In both taxa localized stress peaks are present in the subtemporal and postorbital bars, the quadrate, and in the ventral surface of the pterygoid in all biting positions. Elevated stresses are also observed as a result of bending in the arched nasal region during anterior and, to a lesser extent, midpoint bites in both taxa (Fig. 3). This is particularly apparent in *Plateosaurus*, where a strong peak in compressive stress is observed at

the anterior edge of the base of the premaxillary ascending process (Fig. 3; see also Button *et al.* 2016). In posterior biting elevated stress and some sharp peaks are observed in the suborbital bar, postorbital bar and lacrimal in both taxa, although peak stresses are lower in *Camarasaurus*.

Stress and strain distributions within the mandible differ less between biting positions in both taxa (Fig. 4). In each taxon elevated stress and strain is more widespread in more anterior bites due to the longer moment arm for bending forces resulting from loading of the biting teeth. This is particularly pronounced in *Plateosaurus*, where large stresses and strains are observed along the dorsal and ventral edges of the relatively gracile dentary.

TABLE 6. Results of the analyses replicating bilateral anterior, midpoint and posterior bites in the skull and mandible of *Plateosaurus* and *Camarasaurus*.

	Minimum element stress (MPa)	Mean element stress (MPa)	Maximum element stress (MPa)	Total strain energy (mJ)
Plateosaurus				
Cranium				
Anterior bite	4.36×10^{-10}	1.38	53.10	18.67
Mid bite	2.53×10^{-10}	1.26	32.35	16.06
Posterior bite	8.65×10^{-09}	1.26	567.54	20.91
Mandible				
Anterior bite	3.21×10^{-05}	3.01	54.54	28.54
Mid bite	2.60×10^{-05}	2.56	29.75	22.91
Posterior bite	9.99×10^{-06}	1.50	78.97	8.57
Plateosaurus 'structural comparison'				
Cranium				
Anterior bite	7.54×10^{-10}	2.42	92.85	37.42*
Mid bite	4.41×10^{-10}	2.21	56.63	32.39*
Posterior bite	1.53×10^{-08}	2.20	1025.3	42.03*
Mandible				
Anterior bite	1.40×10^{-03}	6.71	121.75	102.84*
Mid bite	5.80×10^{-05}	5.72	66.42	82.54*
Posterior bite	2.22×10^{-05}	3.36	176.27	30.90*
Camarasaurus				
Cranium				
Anterior bite	8.28×10^{-08}	0.72	19.68	26.31
Mid bite	1.24×10^{-08}	0.77	21.56	28.88
Posterior bite	5.40×10^{-09}	0.80	49.23	28.28
Mandible				
Anterior bite	3.11×10^{-08}	2.16	26.90	52.20
Mid bite	7.55×10^{-09}	1.88	23.98	45.89
Posterior bite	4.82×10^{-09}	1.31	212.32	30.85

Maximum, minimum and mean element von Mises stresses and the total strain energy is given for each analysis. The 'structural comparison' *Plateosaurus* models were scaled so that the ratio between total applied muscle force and the cranium/mandible skull surface area equalled that of the *Camarasaurus* model, so that differences in von Mises stress results between the two will be a result of variance in shape, rather than size or applied muscle force. Strain energy results (*) were further corrected to account for differences in volume between the two taxa, again allowing comparison of performance in terms of shape, rather than size or applied muscle force. See text and Table 1 for more details.

A greater discrepancy is observed between the mandibles of each taxon when loaded under a unilateral bite. High stress peaks are observed in the articular region of *Plateosaurus* (Fig. 5A, B), as compared to *Camarasaurus* (Fig. 5C). After size correction, functionally induced stresses are notably greater in the mandible of *Plateosaurus*, with relatively high stresses along the ventral edges of both the working and balancing sides of the mandible (Fig. 5B, C).

After correcting for differences in size, the total strain energy is also notably lower for both the skull and mandible of *Camarasaurus* than those of *Plateosaurus* at all biting positions (Table 6), particularly so in the mandible during anterior and midpoint bites. An exception to this is in the mandible during a posterior bite, however, where the total strain energy exhibited by both the *Camarasaurus* and *Plateosaurus* models is very similar (Table 6).

DISCUSSION

Myological comparison of Plateosaurus *and* Camarasaurus

One minor rearrangement in jaw musculature occurs between the basally branching sauropodomorph *Plateosaurus* and the neosauropod *Camarasaurus*, in the insertion site of the m.PSTp. The absence of the epipterygoid in neosauropods (Upchurch *et al.* 2004) indicates that, at the very least, the insertion site of this muscle must have shifted, but the absence of any other osteological correlates
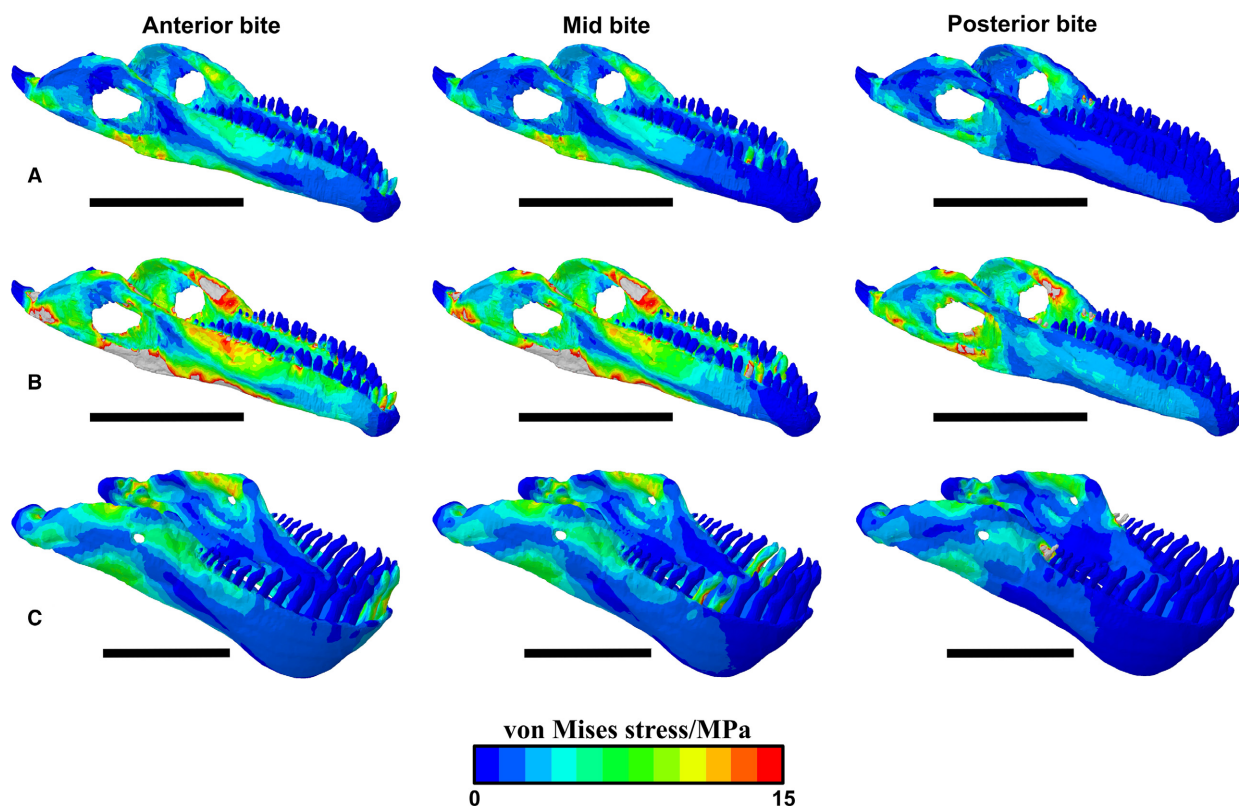
FIG. 4. Von Mises stress contour plots from FEA of the mandibles of *Plateosaurus* and *Camarasaurus* for replicated bilateral anterior (left), midpoint (middle) and posterior (right) bites, in oblique lateral view. A, results for the unscaled *Plateosaurus* model. B, results for *Plateosaurus* when scaled so that the ratio of total applied muscle force:mandible surface area equalled that of *Camarasaurus*, for the 'structural comparison'. C, results for *Camarasaurus*. All scale bars represent 100 mm.

suggests that it was lost altogether (Holliday 2009). Insertion and origination sites for all other adductor muscles remain consistent between the two taxa, but muscle lines of action differ due to changes in overall skull proportions and architecture. Lines of muscle action in *Camarasaurus* are generally more vertical (and so more efficient at driving vertical jaw adduction) than those of *Plateosaurus*, especially with respect to the pterygoideus group (Table 5). Jaw adductor muscle size also differs markedly between the two taxa, in terms of overall and relative muscle volume, and cross-sectional area (Table 4).

After scaling to minimize the influence of skull size, the summed physiological cross-sectional area (proportional to contractile force) of the adductor musculature of *Plateosaurus* is *c.* 57% of that of *Camarasaurus*. Although *Plateosaurus* possesses relatively large origination areas in the supratemporal fossa (Fig. 1A, D) and expansive insertion areas on the mandible (Fig. 1E, F) osteological constraints result in a relatively small, and particularly narrow, adductor chamber (Figs 2, 6). Within sauropods such as *Camarasaurus* these constraints are relaxed by the increase in the relative size of the postorbital region, and the strong transverse expansion of the

skull (cf. Figs 1C, I; 7). The size of the sauropod adductor chamber is further increased due to rearrangement of the palate. In the plesiomorphic sauropodomorph condition, as in *Plateosaurus*, the ectopterygoid sutures to the medial surface of the jugal (Fig. 6A), which tightly constrains the anterior extent of the adductor chamber (Fig. 6B, C). In neosauropods, such as *Camarasaurus*, the ectopterygoid is shifted anteriorly, suturing to the medial surface of the maxilla (Upchurch *et al.* 2004; Fig. 6D), releasing this anterior constraint on the adductor musculature (Fig. 7E, F). In *Plateosaurus* the narrow shape of the skull and the presence of a large pterygoid flange also limit the extent of the adductor musculature (Fig. 1B).

The relative contributions of the different muscle groups to overall muscle volume, and thus bite force, varies between the two taxa, with the pterygoideus group muscles being more important in *Camarasaurus* than *Plateosaurus* (Table 5). This difference is even more striking in the diplodocoid neosauropod *Diplodocus*, where the palatal musculature accounts for >68% of the total jaw adductor force (Button *et al.* 2014). Along with the morphology of the expanded craniomandibular joint, the relative importance of the pterygoideus group muscles in
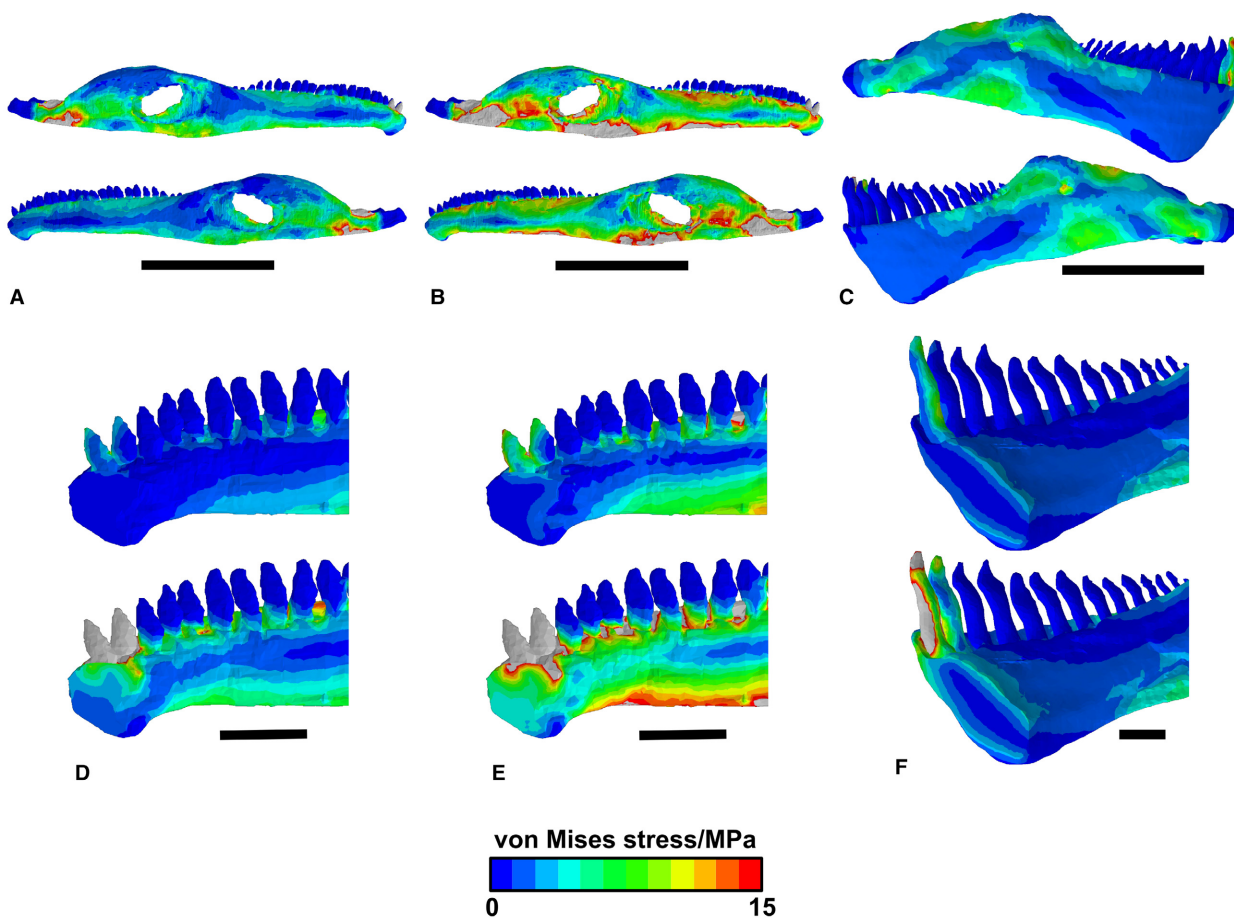
FIG. 5. Von Mises stress contour plots illustrating stresses in the mandible under a unilateral anterior bite, loading the first two teeth of the right tooth row. A, *Plateosaurus* mandible in right (top) and left (bottom) lateral view. B, 'structural comparison' model of the mandible of *Plateosaurus* in right (top) and left (bottom) lateral view. C, *Camarasaurus* mandible in right (top) and left (bottom) lateral view. D–F, contour plots viewed in a sagittal plane taken level with the centre of the mandibular symphysis, for bilateral (top) and unilateral (bottom) bites. Views of the unilateral bites are towards the biting teeth. D, *Plateosaurus*. E, 'structural comparison' *Plateosaurus* model. F, *Camarasaurus*. All scale bars represent 100 mm.

Diplodocus is thought to have enabled translational jaw movements (Barrett & Upchurch 1994; Upchurch & Barrett 2000; Young *et al.* 2012; Button *et al.* 2014). Likewise, the development of more a powerful pterygoideus musculature in sauropods than those present in more basally branching sauropodomorphs may indicate greater reliance on anteroposterior jaw motions, a trait that has evolved on numerous occasions among herbivorous tetrapods (Reisz & Sues 2000; Sues 2000), including multiple times among dinosaurs (e.g. Rybczynski & Vickaryous 2001; Mallon & Anderson 2014; Nabavizadeh 2016; Varriale 2016).

Bite force comparison

Calculated bite forces for *Camarasaurus* greatly exceed those of *Plateosaurus* (Table 5). This reflects both the absolutely and relatively greater adductor muscle mass of *Camarasaurus* (Table 4) and its greater biting efficiency (in terms of the proportion of input muscle force converted to bite force) in comparison to that of *Plateosaurus* (Table 5). Increased bite efficiency is a consequence of changes in jaw shape that result in greater mechanical advantage for most of the adductor muscles in *Camarasaurus*, in particular the expansion of the coronoid eminence, which increases the inlever for the m.AME group. The longer tooth row of *Plateosaurus* results in greater variance in muscle outlevers, and so in bite force and closing speed across the jaw. Within a third-order lever, such as a vertebrate jaw, the mechanical advantage is the inverse of jaw closure speed (Sakamoto 2010). Anterior bites of *Plateosaurus* would have been weak, but relatively fast, whereas posterior bites and bites across the entire tooth row of *Camarasaurus* would have been relatively powerful but slow.

The greater variance in bite force along the jaw of *Plateosaurus* is reflected by tooth morphology. Whereas sauropods such as *Camarasaurus* exhibit homodonty (Upchurch *et al.* 2004) basal sauropodomorph taxa, such as *Plateosaurus*, typically exhibit heterodonty (Barrett 2000; Galton & Upchurch 2004; Barrett & Upchurch 2007). The premaxillary and anteriormost dentary teeth are conical and sometimes slightly recurved (Barrett 2000; Galton & Upchurch 2004; Barrett & Upchurch 2007; Prieto-Márquez & Norell 2011). Their position at the anterior end of the snout (associated with weaker but more rapid bites) is consistent with a suggested role in food procurement, being used to seize or pluck plant and/or animal matter (Barrett 2000). The maxillary and remaining dentary teeth are lanceolate and denticulate (Barrett 2000; Galton & Upchurch 2004; Barrett & Upchurch 2007; Prieto-Márquez & Norell 2011). These 'more herbivorous' posterior teeth would have served to tear and shear procured material (Barrett 2000), consistent with their position in the posterior regions of the tooth row, associated with slower but more forceful bites.

Biomechanical modelling comparison

Finite element modelling demonstrates that functionally induced stresses and strains are greater in both the cranium and mandible of *Plateosaurus* at all tested biting positions, after correcting for size and applied force (Figs 3B, C; 4B, C). As a result, if loading were increased, the skull of *Plateosaurus* would fail first; the cranium and mandible of *Camarasaurus* can hence be considered 'stronger' under static biting. Interestingly, stress magnitudes between *Camarasaurus* and the unscaled *Plateosaurus* are similar, suggesting conservation of similar safety factors when realistic loads are applied. Additionally, the distributions of elevated stress and strain patterns are broadly similar for the two taxa.

Premaxillary and anterior maxillary bites result in elevated stresses in the ascending processes of the premaxillae in both taxa. However, the magnitude of this induced stress is much greater in *Plateosaurus*, which also exhibits elevated stresses in the region surrounding the premaxilla–maxilla suture. Barrett & Upchurch (2007) suggested that slight movements of the premaxilla during biting may have been possible in 'prosauropods' by virtue of a flexible joint at the premaxilla–maxilla suture and that this 'passive kinesis' might have dampened these stresses in a 'shock-absorbing' function, similar to the role of patent sutures in the skull of *Tyrannosaurus rex* (Rayfield 2004). However, more significant movements of the premaxilla are rendered impossible by its immobile contact with the nasals (Barrett & Upchurch 2007; *contra* Gow *et al.* 1990); even if appreciable dorsal rotation was

possible in response to loading this would only increase bending stresses in the delicate premaxillary ascending processes.

Anterior and posterior maxillary bites also result in elevated stresses in the premaxillary ascending processes in *Camarasaurus*, but magnitudes are markedly lower. The retraction of the external naris within Sauropoda leads to the posterodorsal displacement of the relatively fragile ascending processes and expansion of the robust main body of the premaxilla. Elevated stresses are also observed in the very thin sheet of the maxilla forming the wall of the antorbital fossa and the bordering nasals in *Plateosaurus*. However, in *Camarasaurus*, where the antorbital fossa excavates only a small portion of the maxilla and the fenestra is much reduced, these elevated stresses are not observed.

For posterior bites, elevated stresses are observed in the suborbital regions proximate to the biting teeth in both taxa. However, stresses are lower in *Camarasaurus* than *Plateosaurus* due to the shorter tooth row and to the dorsoventral expansion of the cheek region of sauropods relative to the condition in basal sauropodomorph taxa; consequently, the skull of *Camarasaurus* is more robust proximate to the posteriormost biting teeth. Similarly, although elevated stresses are observed in the palates of both taxa, stress magnitudes are much greater in *Plateosaurus*. This results from its more gracile build, as the elongate ectopterygoid shaft accumulates high stresses.

Similarly, although anterior and midpoint bites result in elevated stresses and strains in the dentary due to cantilever bending in the mandibles of both taxa, magnitudes are notably lower in the strongly dorsoventrally expanded dentary of *Camarasaurus*. Total induced stress varies more markedly with changes in bite position in *Plateosaurus* than *Camarasaurus*. This is due both to the more gracile dentary and longer tooth row of *Plateosaurus*. A longer tooth row will result in a greater difference in the moment arm for bending forces, and so induced stresses, resulting from biting at the anteriormost versus the posteriormost teeth.

During anterior and midpoint bites, particularly within the cranium, stresses within the biting teeth are greater in *Plateosaurus* than *Camarasaurus* (Figs 3B, C; 4B–F; 5E–F; 7A–F), with peaks occurring along the lateral surfaces of the tooth crowns. Internal stresses are concentrated within the tooth roots of *Plateosaurus*, with those in the surrounding bone much lower (Fig. 7A, B). In *Camarasaurus* stress is spread more diffusely in the surrounding lateral plate (Fig. 7C–I). This lends support to the hypothesized function of these plates as bracing the teeth (Upchurch & Barrett 2000; see also Young *et al.* 2012), which may have been even more important in lateral tugging or stripping behaviours. However, caution must be applied to interpretations of stress patterns in this region

given the simplistic manner in which the tooth attachments were modelled. The models lack a periodontal ligament, which may influence localized patterns of stress and strain at the base of the teeth (Gröning *et al.* 2011; Wood *et al.* 2011; Fitton *et al.* 2015). Previous sensitivity analyses suggest that inclusion of the periodontal ligament would have resulted in lower stresses in the alveolar bone proximate to the biting tooth (Gröning *et al.* 2011). Finer-scale modelling, including that of hypothetical morphologies, could be used to further investigate the biomechanical significance of this character.

The mandibular symphysis remains relatively unstressed during all tested bilateral biting scenarios (Fig. 5D–F). This is expected given that the constraints on the biting teeth are symmetrical and posterior to the symphysis. In contrast, during unilateral anterior and midpoint bites, stresses are higher in the symphyseal region for both taxa (Fig. 5D–F) as forces are transmitted through it from the working to the balancing side. After correction for size, stresses within the mandibular symphysis of *Plateosaurus* are greater than those of *Camarasaurus* (Fig. 5E, F). This suggests that the expanded mandibular symphysis of sauropods might have been important in accommodating high stresses resulting from asymmetric loading, which is consistent with its previously hypothesized role in strengthening the mandible against feeding-related forces (Barrett & Upchurch 1994;

Upchurch & Barrett 2000; Barrett *et al.* 2007; Upchurch *et al.* 2007). It should be noted, however, that the mandibular symphysis was modelled in a relatively simplistic manner here, and lacked distinct material properties for sutures. Some validation studies have shown that inclusion of sutures within FE models has minimal impact on overall patterns of stress and strain (Bright & Gröning 2011), suggesting that comparisons between models will yield some valid signal. However, it should be noted that work on extant archosaurs has demonstrated that sutures exert a greater impact on the mechanical behaviour of the mandible (Porro *et al.* 2011, 2013; Reed *et al.* 2011; Rayfield 2011). Future work, incorporating sutures, is required to test the behaviour of the mandible in more detail; however, the material properties of archosaur cranial sutures remain poorly known (Porro *et al.* 2013; Cuff *et al.* 2015).

Total strain energy values for the skull of *Camarasaurus* are lower than those for *Plateosaurus* under all tested biting scenarios, and lower in the mandible for anterior and posterior bites. This indicates that the skull of *Camarasaurus* was stiffer than that of *Plateosaurus* and so would have been more efficient at transmitting the force supplied by the adductor musculature (Dumont *et al.* 2009, 2011). This compounds the signal observed in the comparative myology and lever-arm mechanics of these taxa, indicating that *Camarasaurus* was capable of
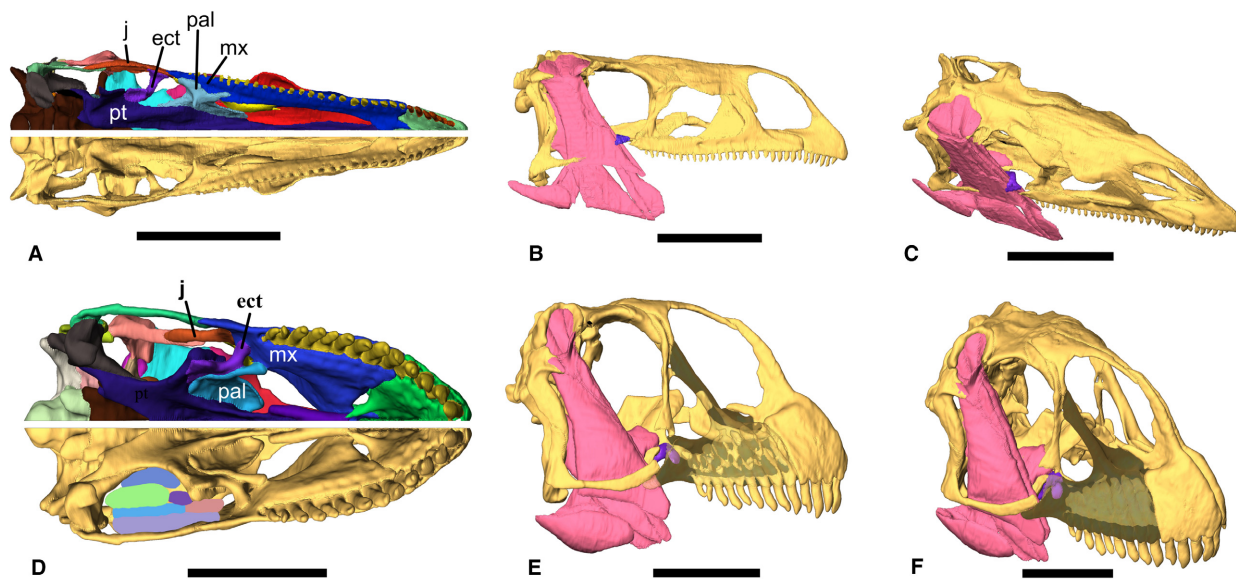

FIG. 6. The constraints upon the jaw adductor musculature provided by the palate in *Plateosaurus* (A–C) and *Camarasaurus* (D–F). A, ventral views of *Plateosaurus* with the right half of the cranium coloured by individual element, and the left half with the jaw adductor muscle bodies depicted as cut along a transect level with the alveolar margin of the skull. B, C, renders of the cranium of *Plateosaurus* with the jugal and postorbital removed; the jaw adductor musculature is indicated in pink and the ectopterygoid in purplej B, right lateral view; C, anterodorsolateral view. D, cranium of *Camarasaurus*, with skull elements and adductor muscles indicated as in A. E, F, cranium of *Camarasaurus* with the jugal and postorbital removed, the maxilla rendered semi-transparent and coloured as in B and C; E, right lateral view; F, anterodorsolateral view. *Abbreviations*: ect, ectopterygoid; j, jugal; mx, maxilla; pal, palate; pt, pterygoid. All scale bars represent 100 mm.

exerting relatively more powerful bites than *Plateosaurus* due to the greater efficiency of the skull and the arrangement and volume of the adductor musculature. Interestingly, however, whereas the mandible of *Plateosaurus* is observed to be inefficient for anterior and midpoint bites, under posterior biting it performs comparably with that of *Camarasaurus* (Table 6). This corroborates the results of lever-arm analysis indicating that the mechanical properties of the jaw of *Plateosaurus* varied considerably across the tooth row, further suggesting some division in role between the anteriormost and posteriormost teeth.

The evolution of herbivory in sauropodomorph dinosaurs

The diversification of sauropodomorph dinosaurs and the evolution of sauropod gigantism have been attributed to the adoption of obligate high-fibre herbivory, and specialization towards bulk-feeding, close to the base of Eusauropoda (Barrett & Upchurch 2007; Upchurch *et al.* 2007; Yates *et al.* 2010; Sander 2013; Barrett 2014). Interpretation of our results in a phylogenetic context (Fig. 8) allows evaluation of these hypotheses through testing of the biomechanical significance of feeding-related characters. However, it should be noted that resolving finer-scale patterns is complicated by the paucity of cranial data from basal sauropodiform taxa and the homoplasy seen in many characters of the feeding apparatus (Barrett & Upchurch 2007; Yates *et al.* 2010). Nevertheless, these results provide perspective on broader functional trends in sauropodomorph cranial evolution.

The retention of an elongate snout and tooth row, despite the resulting compromises in force transmission and 'strength' during anterior bites, suggests that jaw closure speed remained relatively important in *Plateosaurus* and other 'prosauropod' grade taxa. Jaw closure speed is of little importance in herbivory, but is more critical with regards to prey capture. This therefore implies some degree of faunivory, corroborating the anatomical (Barrett 2000; Barrett & Upchurch 2007) and phylogenetic (Barrett *et al.* 2011) arguments for facultative omnivory in basal sauropodomorphs. Indeed, despite being generally considered to have remained morphologically conservative (Barrett & Upchurch 2007; Young & Larvan 2010) the relatively high disparity present in basal sauropodomorph tooth morphology, ranging from recurved teeth in taxa such as *Jingshanosaurus* (Zhang & Yang 1994) to homodont, elongate teeth in *Yunnanosaurus* (Barrett *et al.* 2007) suggests distribution of taxa along the omnivory–herbivory spectrum (Barrett & Upchurch 2007).

Trends in adductor chamber architecture and size are difficult to evaluate in basal sauropodomorph taxa as detailed myological reconstructions are, currently, only available for *Plateosaurus*. Nevertheless, the gross morphology and size of the supratemporal region remains relatively consistent in 'prosauropod' grade taxa, differing primarily in the size of the supratemporal fossa that, although particularly well-developed in *Plateosaurus*, is also present in other taxa (Galton & Upchurch 2004). In all 'prosauropods' the adductor chamber remains relatively vertical and insertion areas on the mandible appear to have remained consistent. However, the size of the coronoid eminence, and so leverage of the m.AME group, is somewhat variable between taxa and may also reflect dietary variation (Barrett & Upchurch 2007).

Comparison of 'prosauropod' and proximate outgroup taxa from which sufficient regions of the palate have been preserved (e.g. *Eoraptor* (Sereno *et al.* 2013), *Pantydraco* (Yates 2003), *Plateosaurus*, *Massospondylus* (Barrett & Yates 2005), *Lufengosaurus* (Barrett *et al.* 2005), *Melanorosaurus* (Yates 2007)) with known sauropod palates (e.g. *Spinophorosaurus* (Remes *et al.* 2009), *Shunosaurus* (Chatterjee & Zheng 2002), *Mamenchisaurus* (Ouyang & He 2002), *Camarasaurus*, *Diplodocus* (Holland 1924), *Euhelopus* (Poropat & Kear 2013), *Sarmientosaurus* (Martínez *et al.* 2016)) allows inference of broad trends. Relative to 'prosauropod' taxa such as *Plateosaurus*, the lateral articulation of the ectopterygoid is shifted more anteriorly to contact the maxilla in sauropods and, possibly, the more basal sauropodiform *Melanorosaurus* (Yates 2007). This is taken further in neosauropods, such as *Camarasaurus*, where the ectopterygoid no longer contacts the jugal and the suborbital fenestra is nearly obliterated (Upchurch *et al.* 2004; Fig. 6). This anterior migration of the ectopterygoid results in anteroposterior expansion of the adductor chamber. This is accentuated further in sauropods by the transverse expansion of the skull and the relative decrease in the size of the preorbital region. This anteroposterior and mediolateral expansion of the adductor chamber permits the greater adductor muscle volume reconstructed in sauropods such as *Camarasaurus* relative to that in 'prosauropods' such as *Plateosaurus*. As well as this increase, the m.PSTp appears to have been lost within Sauropoda at some point along with the epipterygoid (Holliday 2009); an epipterygoid has been reported in *Shunosaurus* (Zheng 1991), *Mamenchisaurus* (Ouyang & He 2002) and *Nebulasaurus* (Xing *et al.* 2015), but appears to have been absent in neosauropods (Upchurch *et al.* 2004).

Immediate outgroups to Sauropoda show the stepwise acquisition of other craniodental characters that have been inferred as related to feeding behaviour (Barrett & Upchurch 2007; Upchurch *et al.* 2007; Fig. 8). These include characters that our finite element models identify as providing greater 'strength' to the skull and mandible with regard to feeding-related loads, including the presence of lateral plates, dorsoventral expansion of the tooth-bearing portion of the mandible and dorsoventral expansion of the mandibular symphysis (see above).
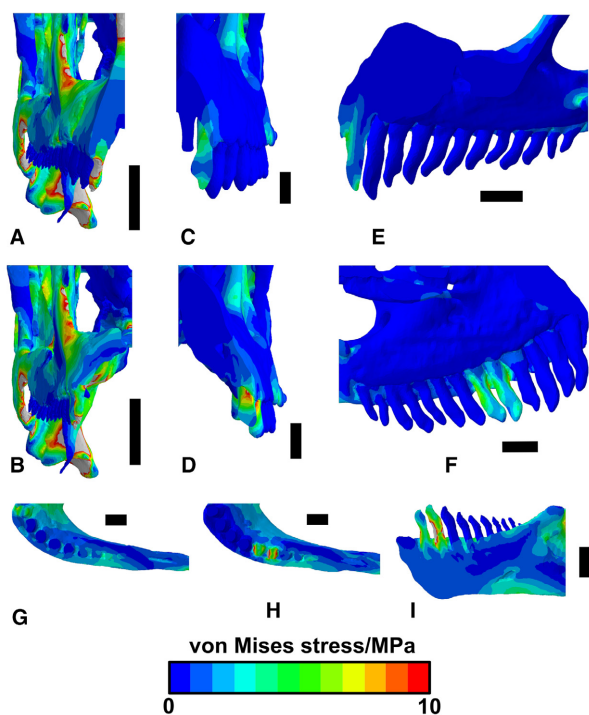
FIG. 7. Von Mises stress contour plots providing a more detailed view of stress in the teeth and surrounding bone of *Plateosaurus* (A, B) and *Camarasaurus* (C–I). A, anterior view of the 'structural comparison' model of *Plateosaurus* under an anterior bite, viewed along a transect through the second premaxillary tooth. B, anterior view of the left half of the skull of the 'structural model' of *Plateosaurus* under a midpoint bite, along a cut through the first maxillary tooth. C, anterior view of *Camarasaurus* under an anterior bite, viewed along a transect taken through the second premaxillary tooth. D, medial view of a transect taken through the middle of the second premaxillary tooth. E, anterior view of the right half of the skull of *Camarasaurus* under a replicated midpoint bite, along a transect taken through the first maxillary tooth. F, medial view of the left maxillary tooth row of *Camarasaurus* under a midpoint bite, showing elevated stress in the medial surface of the lateral plate bracing the teeth. G, dorsal view of the left dentary of *Camarasaurus* under an anterior bite. H, dorsal view of the left dentary of *Camarasaurus* under a midpoint bite. I, medial view of the right dentary of *Camarasaurus* under a midpoint bite, viewed along a cut taken through the fourth premaxillary tooth, showing elevated stress in the medial surface of the lateral plate around the biting teeth. All scale bars represent 20 mm.

Additionally, general trends in cranial morphology occurring at the base of Eusauropoda (the increased breadth of the snout, the increased height of the premaxilla and accompanying posterodorsal deflection of the premaxilla ascending processes, reduction of the antorbital fossa, dorsoventral expansion of the cheek region, and generally more robust build of the skull and mandible) also lower the magnitudes of peak functionally-induced stresses.

The increase in bite force that characterizes the 'prosauropod'–sauropod transition results from an increase in coronoid eminence height, reduction in tooth row length and other changes in shape that result in greater mechanical advantages for the majority of the jaw adductor muscles. An increase in mechanical advantage, and thus bite force at the expense of speed, is typical of herbivorous lineages where jaw closure speed is no longer important (Stayton 2006). This increase in bite force is mirrored by the appearance of characters that facilitated cropping of tough, fibrous plant matter at the expense of oral processing efficiency. These include the development of spatulate tooth crowns, tooth-tooth occlusion, a reduced tooth row, broader snout and the inferred loss of cheeks, which would have allowed a wider gape (Barrett & Upchurch 2007; Upchurch *et al.* 2007). The abbreviation of the tooth row and development of a homodont dentition in sauropods like *Camarasaurus* results in bite mechanics that are more consistent over the length of the jaw, as would be expected in a non-chewing herbivore where the entire tooth row was used in cropping (Christiansen 1999).

These trends towards greater structural strength and increased cropping abilities are consistent with an ecological shift towards generalized bulk-feeding on tough, fibrous plant material (Barrett & Upchurch 2007; Upchurch *et al.* 2007; Yates *et al.* 2010; Sander *et al.* 2011; Sander 2013). Moreover, the functional interrelationships between sequentially acquired myological, osteological and biomechanical characters supports their development under a model of correlated progression (*sensu* Thomson 1966, 1988; Kemp 2007), where functionally integrated characters evolve in a correlated fashion due to positive feedback loops between them (Barrett & Upchurch 2007; Barrett 2014). Under this scenario, the development of more sophisticated adaptations for herbivory (Barrett & Upchurch 2007) and increases in bite force would have allowed the consumption of coarser forage, and the associated increase in feeding-related forces would also support the evolution of structural characters of the skull and mandible.

Similarly, an ecological shift towards obligate herbivory and bulk feeding has been suggested to have driven the evolution of the sauropod *bauplan* through positive feedback loops between cranial and postcranial character complexes (Barrett & Upchurch 2007; Barrett 2014; McPhee *et al.* 2015) or as part of an 'evolutionary cascade' (Sander *et al.* 2011; Sander 2013). In particular, the physical and potential nutritional advantages of large body size for such a dietary strategy (Farlow 1987; Clauss & Hummel 2005; Clauss *et al.* 2013) have led to the adoption of such a habit being invoked as integral to the evolution of sauropod gigantism (Barrett & Upchurch 2007; Upchurch *et al.* 2007; Sander 2013; Barrett 2014).
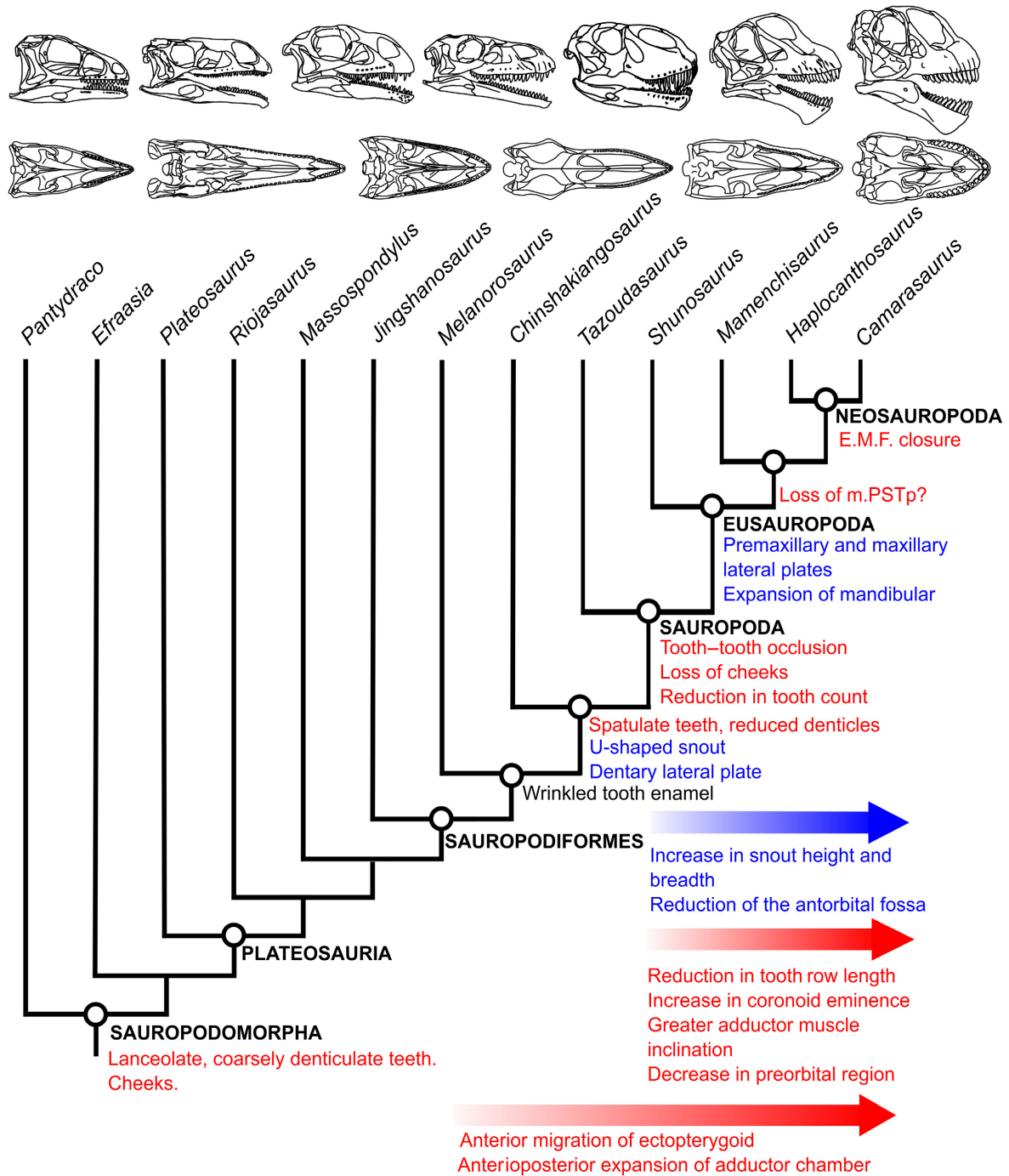
FIG. 8. Simplified phylogeny of the Sauropodomorpha showing the development of the craniodental apparatus. Tree topology after Benson *et al.* (2014) and McPhee *et al.* (2015). Skulls of exemplar taxa illustrated as follows. Left to right: *Pantydraco* in lateral and ventral views (redrawn from Yates (2003)); *Plateosaurus* in lateral and ventral views; *Massospondylus* in lateral view (redrawn from Gow *et al.* (1990)); *Melanorosaurus* in lateral and ventral views (redrawn from Yates (2007)); *Shunosaurus* in lateral and ventral views (redrawn from Chatterjee & Zheng (2002)); *Mamenchisaurus* in lateral and ventral views (redrawn from Ouyang & He (2002)); *Camarasaurus*. Functional characters of the feeding apparatus are mapped onto nodes after Barrett & Upchurch (2007), Upchurch *et al.* (2007) and results presented herein (see Discussion). E.M.F., external mandibular fenestra; m.PSTp, m. pseudotemporalis profundus. Characters found to be primarily associated with cranial robustness in blue, those primarily associated with cropping ability (bite force, tooth form) in red; wrinkled tooth enamel is of uncertain functional significance. Trends in craniodental morphology found by the analyses presented herein to be functionally significant (the increase in adductor chamber size within Sauropodomorpha and numerous shape changes within Sauropodiformes) are indicated and colour-coded as appropriate.

The identification of myological and biomechanical trends within the craniodental apparatus that are consistent with this ecological shift provides support for those scenarios linking an ecological shift to gigantism. However, quantitative comparisons between trends in postcranial character complexes, body size and biomechanical data from a larger sample of sauropodomorph taxa within a rigorous phylogenetic context is still required in order to more thoroughly test these hypotheses.

CONCLUSIONS

Myological reconstructions of the jaw adductor musculature in the 'prosauropod' *Plateosaurus* and the neosauropod *Camarasaurus* indicate greater muscle masses in the latter, with modifications of the skull and palate that allow expansion of the adductor chamber. Calculated bite forces for *Camarasaurus* are also much greater, due both to increased muscle mass and greater mechanical advantage of the jaw adductor musculature. Finite element modelling demonstrates that the skull and mandible of *Camarasaurus* are both more mechanically efficient and 'stronger' under loading replicating static biting than *Plateosaurus*. This is primarily a consequence of the generally more robust build of cranial elements in *Camarasaurus*. Modelling also demonstrates the biomechanical significance of some sauropod synapomorphies including shape changes in the snout and the lateral plates. These appear to dissipate stresses in the biting teeth and the expanded mandibular symphysis, which may have been particularly important under asymmetric loading. Further modelling studies involving theoretical morphologies and introducing more compliant cranial suture tissues could be used to more thoroughly test the significance of these characters.

Placing these results in a phylogenetic context indicates morphological trends that result in greater bite forces and increased cranial robustness close to the base of Sauropoda, coincident with the development of more 'herbivorous' adaptations of the teeth. These trends provide biomechanical evidence for the hypothesized shift towards bulk-feeding and obligate herbivory at the base of Sauropoda. The functional linkages present between these characters suggest that this ecological shift drove the evolution of these disparate characters through correlated-progression, with positive feedback loops precipitating a functional complex adapted towards the exertion and accommodation of greater forces. The coincidence of this ecological shift with those in various aspects of sauropodomorph anatomy suggests that dietary evolution drove the evolution of postcranial characters and ultimately sauropod gigantism in a similar manner, although comparisons between the appearance of cranial characters with evolutionary trends in body mass and the postcranial skeleton are required to test this further.

DATA ARCHIVING STATEMENT

Data for this study are available in the Dryad Digital Repository: http://dx.doi.org/10.5061/dryad.vr954

Editor. Roger Benson

REFERENCES

BARRETT, P. M. 2000. Prosauropods and iguanas: speculation on the diets of extinct reptiles. 42–78. *In* SUES, H.-D. (ed.) *The evolution of herbivory in terrestrial vertebrates: perspectives from the fossil record.* Cambridge University Press.

—— 2014. Paleobiology of herbivorous dinosaurs. *Annual Review of Earth & Planetary Sciences*, **42**, 207–230.

—— and RAYFIELD, E. J. 2006. Ecological and evolutionary implications of dinosaur feeding behaviour. *Trends in Ecology & Evolution*, **21**, 218–224.

—— and UPCHURCH, P. 1994. Feeding mechanisms of *Diplodocus. Gaia*, **10**, 195–204.

—— —— 2005. Sauropodomorph diversity through time: macroevolutionary and paleoecological implications. 125–156. *In* CURRY ROGERS, K. A. and WILSON, J. A. (eds). *The sauropods: evolution and paleobiology.* University of California Press.

—— —— 2007. The evolution of feeding mechanisms in early sauropodomorph dinosaurs. *Special Papers in Palaeontology*, **77**, 91–112.

—— and YATES, A. M. 2005. New information on the palate and lower jaw of *Massospondylus* (Dinosauria: Sauropodomorpha). *Palaeontologia Africana*, **41**, 123–130.

—— UPCHURCH, P. and XIAOLIN, W. 2005. Cranial osteology of *Lufengosaurus huenei* Young (Dinosauria: Prosauropoda) from the Lower Jurassic of Yunnan, People's Republic of China. *Journal of Vertebrate Paleontology*, **25**, 806–822.

—— —— ZHOU, X. D. and WANG, X. 2007. The skull of *Yunnanosaurus huangi* Young, 1942 (Dinosauria: Prosauropoda) from the Lower Lufeng Formation (Lower Jurassic) of Yunnan, China. *Zoological Journal of the Linnean Society*, **150**, 319–341.

—— BUTLER, R. J. and NESBITT, S. J. 2011. The roles of herbivory and omnivory in early dinosaur evolution. *Earth & Environmental Science Transactions of the Royal Society of Edinburgh*, **101**, 383–396.

BATES, K. T., FALKINGHAM, P. L., MACAULAY, S., BRASSEY, C. and MAIDMENT, S. C. R. 2015. Downsizing a giant: re-evaluating *Dreadnoughtus* body mass. *Biology Letters*, **11**, 20150215.

BENSON, R. B. J., CAMPIONE, N. E., CARRANO, M. T., MANNION, P. D., SULLIVAN, C., UPCHURCH, P. and EVANS, D. C. 2014. Rates of dinosaur body mass evolution indicate 170 million years of sustained ecological innovation on the avian stem lineage. *PLoS One*, **12**, e1001853.

BRIGHT, J. A. 2014. A review of paleontological finite element models and their validity. *Journal of Paleontology*, **88**, 760–769.

—— and GRÖNING, F. 2011. Strain accommodation in the zygomatic arch of the pig: a validation study using digital speckle pattern interferometry and finite element analysis. *Journal of Morphology*, **272**, 1388–1398.

—— and RAYFIELD, E. J. 2011. Sensitivity and *ex vivo* validation of finite element models of the domestic pig cranium. *Journal of Anatomy*, **219**, 456–471.

BUTTON, D. J., RAYFIELD, E. J. and BARRETT, P. M. 2014. Cranial biomechanics underpins high sauropod diversity in resource-poor environments. *Proceedings of the Royal Society B*, **281**, 20142114.

—— BARRETT, P. M. and RAYFIELD, E. J. 2016. Data from: Comparative cranial myology and biomechanics of *Plateosaurus* and *Camarasaurus* and evolution of the sauropod feeding apparatus. *Dryad Digital Repository*. doi: 10.5061/dryad.vr954

CALVO, J. O. 1994. Jaw mechanics in sauropod dinosaurs. *Gaia*, **10**, 183–193.

CHAPMAN, J. E. and REISS, M. J. 1999. *Ecology: principles and applications*, 2nd edn. Cambridge University Press, 335 pp.

CHATTERJEE, S. and ZHENG, Z. 2002. Cranial anatomy of *Shunosaurus*, a basal sauropod dinosaur from the Middle Jurassic of China. *Zoological Journal of the Linnean Society*, **136**, 145–169.

CHRISTIANSEN, P. 1999. On the head size of sauropodomorph dinosaurs: implications for ecology and physiology. *Historical Biology*, **13**, 269–297.

—— 2000. Feeding mechanisms of the sauropod dinosaurs *Brachiosaurus*, *Camarasaurus*, *Diplodocus* and *Dicraeosaurus*. *Historical Biology*, **14**, 137–152.

CHURE, D., BRITT, B. B., WHITLOCK, J. A. and WILSON, J. A. 2010. First complete sauropod dinosaur skull from the Cretaceous of the Americas and the evolution of sauropod dentition. *Naturwissenschaften*, **97**, 379–391.

CLAUSS, M. 2011. Sauropod biology and the evolution of gigantism: what do we know? 3–10. *In* KLEIN, N., REMES, K., GEE, C. T. and SANDER, P. M. (eds). *Biology of the sauropod dinosaurs: understanding the life of giants*. Indiana University Press.

—— and HUMMEL, J. 2005. The digestive performance of mammalian herbivores: why big may not be that much better. *Mammal Review*, **35**, 174–187.

—— STEUER, P., MÜLLER, D. W. H., CODRON, D. and HUMMEL, J. 2013. Herbivory and body size: allometries of diet quality and gastrointestinal physiology, and implications for herbivore ecology and dinosaur gigantism. *PLoS One*, **8**, e68714.

COLBERT, E. H. 1993. Feeding strategies and metabolism in elephants and sauropod dinosaurs. *American Journal of Science*, **293A**, 1–19.

CORIA, R. A. and CURRIE, P. J. 2002. The braincase of *Giganotosaurus carolinii* (Dinosauria: Theropoda) from the Upper Cretaceous of Argentina. *Journal of Vertebrate Paleontology*, **22**, 802–811.

CUFF, A. R. and RAYFIELD, E. J. 2015. Retrodeformation and muscular reconstruction of ornithomimosaurian dinosaur crania. *PeerJ*, **3**, 31093.

—— BRIGHT, J. and RAYFIELD, E. J. 2015. Validation experiments on finite element models of an ostrich (*Struthio camelus*) cranium. *PeerJ*, **3**, e1294.

CURRY, K. A. 1999. Ontogenetic histology of *Apatosaurus* (Dinosauria: Sauropoda): new insights on growth rates and longevity. *Journal of Vertebrate Paleontology*, **19**, 654–665.

DUMONT, E. R., GROSSE, I. R. and SLATER, G. J. 2009. Requirements for comparing the performance of finite element models of biological structures. *Journal of Theoretical Biology*, **256**, 96–103.

—— DAVID, J. L., GROSSE, I. L. and BURROWS, A. M. 2011. Finite element analysis of performance in the skulls of marmosets and tamarins. *Journal of Anatomy*, **218**, 151–162.

EIJDEN, T. M. G. J. VAN, KORFAGE, J. A. M. and BRUGMAN, P. 1997. Architecture of the human jaw-closing and jaw-opening muscles. *The Anatomical Record*, **248**, 464–474.

FAIRMAN, J. E. 1999. Prosauropod and iguanid jaw musculature: a study on the evolution of form and function. Unpublished MSc thesis, John Hopkins University, 95 pp.

FARLOW, J. O. 1987. Speculations about the diet and digestive physiology of herbivorous dinosaurs. *Paleobiology*, **13**, 60–72.

FITTON, L. C., PRÔA, M., ROWLAND, C., TORO-IBACACHE, V. and O'HIGGINS, P. 2015. The impact of simplifications on the performance of a finite element model of a *Macaca fascicularis* cranium. *The Anatomical Record*, **298**, 107–121.

GALTON, P. M. 1985a. Diet of prosauropod dinosaurs from the late Triassic and early Jurassic. *Lethaia*, **18**, 105–123.

—— 1985b. Cranial anatomy of the prosauropod dinosaur *Plateosaurus* from the Knollenmergel (Middle Keuper, Upper Triassic) of Germany. II. All the cranial material and details of soft-part anatomy. *Geologica et Palaeontologica*, **19**, 119–159.

—— and UPCHURCH, P. 2004. Prosauropoda. 232–258. *In* WEISHAMPEL, D. B., DODSON, P. and OSMÓLSKA, H. (eds). *The Dinosauria*, 2nd edn. University of California Press.

GILMORE, R. S., POLLACK, R. P. and KATZ, J. L. 1969. Elastic properties of bovine dentine and enamel. *Archives of Oral Biology*, **15**, 787–796.

GOW, C. E., KITCHING, J. W. and RAATH, M. A. 1990. Skulls of the prosauropod dinosaur *Massospondylus carinatus* Owen in the collections of the Bernard Price

Institute for Palaeontological Research. *Palaeontologia Africana*, **27**, 45–58.

GRÖNING, F., FAGAN, M. J. and O'HIGGINS, P. 2011. The effects of the periodontal ligament on mandibular stiffness: a study combining finite element analysis and geometric morphometrics. *Journal of Biomechanics*, **44**, 1304–1312.

HAAS, G. 1963. A proposed reconstruction of the jaw musculature of *Diplodocus*. *Annals of the Carnegie Museum*, **36**, 139–157.

HATCHER, J. B. 1901. *Diplodocus* (Marsh): its osteology, taxonomy, and probable habits, with a restoration of the skeleton. *Memoirs of the Carnegie Museum of Natural History*, **1**, 1–63.

HOLLAND, W. J. 1924. The skull of *Diplodocus*. *Memoirs of the Carnegie Museum*, **9**, 379–403.

HOLLIDAY, C. M. 2009. New insights into dinosaur jaw muscle anatomy. *The Anatomical Record*, **292**, 1246–1265.

—— and WITMER, L. M. 2007. Archosaur adductor chamber evolution: integration of musculoskeletal and topological criteria in jaw muscle homology. *Journal of Morphology*, **268**, 457–484.

—— TSAI, H. P., SKILJAN, R. J., GEORGE, I. D. and PATHAN, S. 2013. A 3D interactive model and atlas of the jaw musculature of *Alligator mississippiensis*. *PLoS One*, **8**, e62806.

HUMMEL, J. and CLAUSS, M. 2011. Sauropod feeding and digestive physiology. 11–33. *In* KLEIN, N., REMES, K., GEE, C. T. and SANDER, P. M. (eds). *Biology of the sauropod dinosaurs: understanding the life of giants*. Indiana University Press.

ICHIM, I., SCHMIDLIN, P. R., KIESER, J. A. and SWAIN, M. V. 2007. Mechanical evaluation of cervical glass-ionomer restorations: 3D finite element study. *Journal of Dentistry*, **35**, 28–35.

IKEJIRI, T., TIDWELL, V. and TREXLER, D. L. 2005. New adult specimens of *Camarasaurus lentus* highlight ontogenetic variation within the species. 154–179. *In* CARPENTER, K. and TIDWELL, V. (eds). *Thunder-lizards: the sauropodomorph dinosaurs*. University of Indiana Press.

KEMP, T. S. 2007. The concept of correlated progression as the basis of a model for the evolutionary origin of major new taxa. *Proceedings of the Royal Society B*, **274**, 1667–1673.

KLEIN, N., REMES, K., GEE, C. T. and SANDER, P. M. (eds). 2011. *Biology of the sauropod dinosaurs: understanding the life of giants*. Indiana University Press, 331 pp.

LACOVARA, K. J., LAMANNA, M. C., IBIRICU, L. M., POOLE, J. C., SCHROETER, E. R., ULLMANN, P. V., VOEGELE, K. K., BOLES, Z. M., CARTER, A. M., FOWLER, E. K., EGERTON, V. M., MOYER, A. E., COUGHENOUR, C. L., SCHEIN, J. P., HARRIS, J. D., MARTÍNEZ, R. D. and NOVAS, F. E. 2014. A gigantic, exceptionally complete titanosaurian sauropod dinosaur from Southern Patagonia, Argentina. *Scientific Reports*, **4**, 6196.

LAUTENSCHLAGER, S. 2013. Cranial myology and bite force performance of *Erlikosaurus andrewsi*: a novel approach for digital muscle reconstructions. *Journal of Anatomy*, **222**, 260–272.

—— WITMER, L. M., ALTANGEREL, P., ZANNO, L. E. and RAYFIELD, E. J. 2014. Cranial anatomy of *Erlikosaurus andrewsi* (Dinosauria, Therizinosauria): new insights based on digital reconstruction. *Journal of Vertebrate Paleontology*, **34**, 1263–1291.

—— BRASSEY, C. A., BUTTON, D. J. and BARRETT, P. M. 2016. Decoupled form and function in disparate herbivorous dinosaur clades. *Scientific Reports*, **6**, 26495.

MADSEN, J. H. Jr, McINTOSH, J. S. and BERMAN, D. S. 1995. Skull and atlas-axis complex of the Upper Jurassic sauropod *Camarasaurus* (Reptilia: Saurischia). *Bulletin of Carnegie Museum of Natural History*, **31**, 1–115.

MALLON, J. C. and ANDERSON, J. S. 2014. The functional and palaeoecological implications of tooth morphology and wear for the megaherbivorous dinosaurs from the Dinosaur Park Formation (Upper Campanian) of Alberta, Canada. *PLoS One*, **9**, e98605.

MANNION, P. D., UPCHURCH, P., CARRANO, M. T. and BARRETT, P. M. 2011. Testing the effect of the rock record on diversity: a multidisciplinary approach to elucidating the generic richness of sauropodomorph dinosaurs through time. *Biological Reviews*, **86**, 157–181.

MARTÍNEZ, R. D. F., LAMANNA, M. C., NOVAS, F. E., RIDGLEY, R. C., CASAL, G. A., MARTÍNEZ, J. E., VITA, J. R. and WITMER, L. M. 2016. A basal lithostrotian titanosaur (Dinosauria: Sauropoda) with a complete skull: implications for the evolution and paleobiology of Titanosauria. *PLoS One*, **11**, e0151661.

MAZZETTA, G. V., CHRISTIANSEN, P. and FARIÑA, R. A. 2004. Giants and bizarres: body size of some southern South American Cretaceous dinosaurs. *Historical Biology*, **16**, 1–13.

McPHEE, B. W., BONNAN, M. F., YATES, A. M., NEVELING, J. and CHOINIERE, J. 2015. A new basal sauropod from the pre-Toarcian Jurassic of South Africa: evidence of niche-partitioning at the sauropodomorph–sauropod boundary? *Scientific Reports*, **5**, 13224.

MOLNAR, R. E. 2008. Reconstruction of jaw musculature of *Tyrannosaurus rex*. 254–281. *In* LARSON, P. and CARPENTER, K. (eds). *Tyrannosaurus rex*. Indiana University Press.

NABAVIZADEH, A. 2016. Evolutionary trends in the jaw adductor mechanics of ornithischian dinosaurs. *The Anatomical Record*, **299**, 271–294.

OUYANG, H. and HE, Y. 2002. *The first mamenchisaurian skeleton with complete skull:* Mamenchisaurus youngi. Sichuan Science and Technology Press, Chengdu, China, 111 pp. [In Chinese, with English summary]

OWEN-SMITH, N. 1988. *Megaherbivores: the influence of large body size on ecology*. Cambridge University Press, 369 pp.

POROPAT, S. F. and KEAR, B. P. 2013. Photographic atlas and three-dimensional reconstruction of the holotype skull of *Euhelopus zdanskyi* with description of additional cranial elements. *PLoS One*, **8**, e79932.

PORRO, L. B., HOLLIDAY, C. M., ANAPOL, F., ONTIVEROS, L. C., ONTIVEROS, L. T. and ROSS, C. F. 2011. Free body analysis, beam mechanics, and finite element modeling of *Alligator mississippiensis*. *Journal of Morphology*, **272**, 910–937.

—— METZGER, K. A., IRIARTE-DIAZ, J. and ROSS, C. F. 2013. *In vivo* bone strain and finite element modeling of

the mandible of *Alligator mississippiensis*. *Journal of Anatomy*, **223**, 195–227.

PREUSCHOFT, H. and WITZEL, U. 2005. Finite element model construction for the virtual synthesis of skulls in vertebrates: case study of *Diplodocus*. *The Anatomical Record*, **283A**, 391–401.

PRIETO-MÁRQUEZ, A. and NORELL, M. A. 2011. Redescription of a nearly complete skull of *Plateosaurus* (Dinosauria: Sauropodomorpha) from the Late Triassic of Trossingen (Germany). *American Museum Novitates*, **3727**, 1–58.

RAYFIELD, E. J. 2004. Cranial mechanics and feeding in *Tyrannosaurus rex*. *Proceedings of the Royal Society B*, **271**, 1451–1459.

—— 2007. Finite element analysis and understanding the biomechanics and evolution of living and fossil organisms. *Annual Review of Earth & Planetary Sciences*, **35**, 541–576.

—— 2011. Strain in the ostrich mandible during simulated pecking and validation of specimen-specific finite element models. *Journal of Anatomy*, **218**, 47–58.

REED, D. A., PORRO, L. B., IRIATE-DIAZ, J., LEMBERG, J. B., HOLLIDAY, C. M., ANAPOL, F. and ROSS, C. F. 2011. The impact of bone and suture material properties on mandibular function in *Alligator mississippiensis*: testing theoretical phenotypes with finite element analysis. *Journal of Anatomy*, **218**, 59–74.

REICHEL, M. 2010. A model for the bite mechanics in the herbivorous dinosaur *Stegosaurus* (Ornithischia, Stegosauridae). *Swiss Journal of Geoscience*, **103**, 235–240.

REILLY, D. and BURSTEIN, A. 1975. The elastic and ultimate properties of compact bone tissue. *Journal of Biomechanics*, **8**, 393–405.

REISZ, R. R. and SUES, H.-D. 2000. Herbivory in late Paleozoic and Triassic terrestrial vertebrates. 9–42. *In* SUES, H.-D. (ed.) *Evolution of herbivory in terrestrial vertebrates: perspectives from the fossil record*. Cambridge University Press.

REMES, K., ORTEGA, F., FIERRO, I., JOGER, U., KOSMA, R., FERRER, J. M. M., PALDES, S. N. H. M., IDE, O. A. and MAGA, A. 2009. A new basal sauropod dinosaur from the Middle Jurassic of Niger and the early evolution of Sauropoda. *PLoS One*, **4**, e6924.

RYBCZYNSKI, N. and VICKARYOUS, M. K. 2001. Evidence of complex jaw movement in the Late Cretaceous ankylosaurid *Euoplocephalus tutus* (Dinosauria: Thyreophora). 299–317. *In* CARPENTER, K. (ed.) *The armored dinosaurs*. Indiana University Press.

SAKAMOTO, M. 2010. Jaw mechanics and the evolution of biting performance in theropod dinosaurs. *Proceedings of the Royal Society B*, **277**, 3327–3333.

SANDER, P. M. 2013. An evolutionary cascade model for sauropod dinosaur gigantism - overview, update and tests. *PLoS One*, **8**, e78573.

—— and CLAUSS, M. 2008. Sauropod gigantism. *Science*, **322**, 200–201.

—— CHRISTIAN, A., CLAUSS, M., FECHNER, R., GEE, C. T., GRIEBELER, E.-M., GUNGA, H.-C., HUMMEL, J., MALLISON, H., PERRY, S. F., PREUSCHOFT, H., RAUHUT, O. W. M., REMES, K., TÜTKEN, T., WINGS, O. and WITZEL, U. 2011.

Biology of the sauropod dinosaurs: the evolution of gigantism. *Biological Reviews*, **86**, 117–155.

SCHWENK, K. 2000. *Feeding: form, function and evolution in tetrapod vertebrates*. Academic Press, 564 pp.

SERENO, P. C. and DONG, Z. 1992. The skull of the basal stegosaur *Huayangosaurus taibaii* and a cladistic diagnosis of stegosauria. *Journal of Vertebrate Paleontology*, **12**, 318–343.

—— WILSON, J. A., WITMER, L. M., WHITLOCK, J. A., MAGA, A., IDE, O. and ROWE, T. A. 2007. Structural extremes in a Cretaceous dinosaur. *PLoS One*, **2**, e1230.

—— RICARDO, N. M. and ALCOBER, O. A. 2013. Osteology of *Eoraptor lunensis* (Dinosauria: Sauropodomorpha). *Memoirs of the Society of Vertebrate Paleontology*, **12**, 83–179.

STAYTON, C. T. 2006. Testing hypotheses of convergence with multivariate data: morphological and functional convergence among herbivorous lizards. *Evolution*, **60**, 824–841.

STRAIT, D. S., WANG, Q., DECHOW, P. C., ROSS, C. F., RICHMOND, B. G., SPENCER, M. A. and PATEL, B. A. 2005. Modeling elastic properties in finite element analysis: how much precision is needed to produce an accurate model? *The Anatomical Record*, **283**, 275–287.

SUES, H.-D. 2000. Herbivory in terrestrial vertebrates: an introduction. 1–8. *In* SUES, H.-D. (ed.) *Evolution of herbivory in terrestrial vertebrates: perspectives from the fossil record*. Cambridge University Press.

THOMASON, J. J. 1991. Cranial strength in relation to estimated biting forces in some mammals. *Canadian Journal of Zoology*, **69**, 2326–2333.

—— RUSSELL, A. P. and MORGELI, M. 1990. Forces of biting, body size, and masticatory muscle tension in the opossum *Didelphis virginiana*. *Canadian Journal of Zoology*, **68**, 318–324.

THOMSON, K. S. 1966. The evolution of the tetrapod middle ear in the rhipidistian-amphibian transition. *American Zoologist*, **6**, 379–397.

—— 1988. *Morphogeneis and evolution*. Oxford University Press, 154 pp.

TSAI, H. P. and HOLLIDAY, C. M. 2011. Ontogeny for the alligator cartilage transiliens and its significance to sauropsid jaw muscle evolution. *PLoS One*, **6**, e24935.

UPCHURCH, P. and BARRETT, P. M. 2000. The evolution of sauropod feeding mechanisms. 79–122. In: SUES, H.-D. (ed.) *Evolution of herbivory in terrestrial vertebrates: perspectives from the fossil record*. Cambridge University Press.

—— —— and DODSON P. 2004. Sauropoda. 259–322. *In* WEISHAMPEL, D. B., DODSON, P. and OSMÓLSKA, H. (eds). *The Dinosauria*, 2nd edn. University of California Press.

—— —— XIJIN, Z. and XING, X. 2007. A re-evaluation of *Chinshakiangosaurus chunghoensis* Ye *vide* Dong 1992 (Dinosauria, Sauropodomorpha): implications for cranial evolution in basal sauropod dinosaurs. *Geological Magazine*, **144**, 247–262.

VARRIALE, F. J. 2016. Dental microwear reveals mammal-like chewing in the ceratopsian dinosaur *Leptoceratops gracilis*. *PeerJ*, **4**, e2132.

WEISHAMPEL, D. B., BARRETT, P. M., CORIA, R. A., LE LOEUFF, J., XU, X., ZHAO, X., SAHNI, A.,

GOMANI, E. M. P. and NOTO, C. R. 2004. Dinosaur distribution. 517–606. *In* WEISHAMPEL, D. B., DODSON, P. and OSMÓLSKA, H. (eds). *The Dinosauria*, 2nd edn. University of California Press.

WESTNEAT, M. W. 1994. Transmission of force and velocity in the feeding mechanisms of labrid fishes (Teleostei, Perciformes). *Zoomorphology*, **114**, 103–118.

WITMER, L. M. 1995. The extant phylogenetic bracket and the importance of reconstructing soft tissues in fossils. 19–33. *In* THOMASON, J. J. (ed.) *Functional morphology in vertebrate paleontology*. Cambridge University Press.

—— 1997. The evolution of the antorbital cavity of archosaurs: a study in soft-tissue reconstruction in the fossil record with an analysis of the function of pneumaticity. *Memoirs of the Society of Vertebrate Paleontology*, **3**, 1–73.

WITZEL, U., MANNHARDT, J., GOESSLING, R., MICHELI, P. DE and PREUSCHOFT, H. 2011. Finite element analyses and virtual syntheses of biological structures and their application to sauropod skulls. 171–181. *In* KLEIN, N., REMES, K., GEE, C. T. and SANDER, P. M. (eds). *Biology of the sauropod dinosaurs: understanding the life of giants*. Indiana University Press.

WOOD, S. A., STRAIT, D. S., DUMONT, E. R., ROSS, C. F. and GROSSE, I. R. 2011. The effects of modelling simplifications on craniofacial finite element models: the alveoli (tooth sockets) and periodontal ligaments. *Journal of Biomechanics*, **44**, 1831–1838.

XING, L., MIYASHITA, T., CURRIE, P. J., YOU, H., ZHANG, J. and DONG, Z. 2015. A new basal eusauropod from the Middle Jurassic of Yunnan, China, and faunal compositions and transitions of Asian sauropodomorph dinosaurs. *Acta Palaeontologica Polonica*, **60**, 145–154.

YATES, A. M. 2003. A new species of the primitive dinosaur *Thecodontosaurus* (Saurischia: Sauropodomorpha) and its implications for the systematics of early dinosaurs. *Journal of Systematic Palaeontology*, **1**, 1–42.

—— 2007. The first complete skull of the Triassic dinosaur *Melanorosaurus* Haughton (Sauropodomorpha: Anchisauria). *Special Papers in Palaeontology*, **77**, 9–55.

—— BONNAN, M. F., NEVELING, J., CHINSAMY, A. and BLACKBEARD, M. G. 2010. A new transitional sauropodomorph dinosaur from the Early Jurassic of South Africa and the evolution of sauropod feeding and quadrupedalism. *Proceedings of the Royal Society B*, **277**, 787–794.

YOUNG, M. T. and LARVAN, M. D. 2010. Macroevolutionary trends in the skull of sauropodomorph dinosaurs – the largest terrestrial animals to have ever lived. 259–269. *In* ELEWA, A. M. T. (ed.) *Morphometrics for nonmorphometricians*. Springer-Verlag.

—— RAYFIELD, E. J., HOLLIDAY, C. M., WITMER, L. M., BUTTON, D. J., UPCHURCH, P. and BARRETT, P. M. 2012. Cranial biomechanics of *Diplodocus* (Dinosauria, Sauropoda): testing hypotheses of feeding behaviour in an extinct megaherbivore. *Naturwissenschaften*, **99**, 637–643.

ZHANG, Y. and YANG, Z. 1994. *A new complete osteology of Prosauropoda in Lufeng Basin Yunnon China: Jinghsanosaurus*. Yunnan Publishing House of Science and Technology, Kunming, 100 pp. [Chinese with English summary]

ZHENG, Z. 1991. Morphology of the braincase of *Shunosaurus*. *Vertebrata Palasiatica*, **29**, 108–118. [In Chinese, with English summary]